Journal of Environmental Chemical Engineering 11 (2023) 109180

Contents lists available at ScienceDirect

Journal of Environmental Chemical Engineering

journal homepage: www.elsevier.com/locate/jece

Isotherm, kinetics, thermodynamics and mechanism of metal ions adsorption from electroplating wastewater using treated and functionalized carbon nanotubes

Ambali Saka Abdulkareem [a,f], Wasiu Abidemi Hamzat [a,e,f], Jimoh Oladejo Tijani [b,f], Titus Chinedu Egbosiuba [c,f,*], Saheed Mustapha [b,f], Oladiran Kamardeen Abubakre [d,f], Blessing Onyinye Okafor [c], Akinpelu Kamoru Babayemi [c]

[a] Department of Chemical Engineering, Federal University of Technology, P.M.B 65, Minna, Niger State, Nigeria
[b] Department of Chemistry, Federal University of Technology, P.M.B 65, Minna, Niger State, Nigeria
[c] Department of Chemical Engineering, Chukwuemeka Odumegwu Ojukwu University, P.M.B 02, Uli Campus, Anambra State, Nigeria
[d] Department of Mechanical Engineering, Federal University of Technology, P.M.B 65, Minna, Niger State, Nigeria
[e] Department of Chemical Engineering, Carl Von Ossietzky University of Oldenburg, Lowe Saxony, Germany
[f] Nanotechnology Research Group, African Centre for Excellence on Mycotoxin, Federal University of Technology, P.M.B 65, Minna, Niger State, Nigeria

ARTICLE INFO

Editor: Dong-Yeun Koh

Keywords:
Heavy metals
Carbon nanotubes
Wastewater treatment
Adsorption models
Adsorption mechanism

ABSTRACT

The pollution of the environment emanating from the electroplating wastewater containing cadmium, copper, iron, nickel and lead is a universal critical issue that require efficient treatment methods. Herein, super carbon nanotubes (CNTs) were synthesized on iron-nickel/kaolin catalyst, treated (TR-CNTs) and functionalized (PN@TR-CNTs) as a suitable nanoadsorbent. The nanoadsorbents were characterized to confirm the properties by several physicochemical methods such as x-ray diffraction, Fourier transform infrared spectroscopy, high resolution scanning electron microscopy, high-resolution transmission electron microscopy, energy dispersive x-ray and Brunauer–Emmett–Teller. The characterizations indicate successful synthesis, purification and functionalization of the nanoadsorbents. The surface area of the CNTs, TR-CNTs and PN@TR-CNTs were evaluated as 583.31, 781.88 and 970.81 $m^2\ g^{-1}$, respectively. The effect of pH, contact time, nanoadsorbent dosage and temperature on the adsorption of the selected metal ions was carried out and the best conditions were obtained at pH (5 and 6), contact time (60 min), nanoadsorbent dosage (0.4 g/L) and temperature (50 °C). Redlich-Peterson and pseudo second-order isotherm and kinetic models best fitted the experimental data. Similarly, the metal ions adsorption by TR-CNTs and PN@TR-CNTs were thermodynamically spontaneous. The adsorption mechanism was dominated by pore filling and electrostatic attraction, ahead of hydrogen bonding and surface complexation. With good reusability of 6 cycles, the nanoadsorbents can be utilized as a potential material for metal ions removal from electroplating wastewater.

1. Introduction

Water is one of the most important natural resources for maintaining human life. Several pollutants such as heavy metals, dyes and antibiotics are regrettably entering natural water systems due to increased population growth and industrialization [1]. For instance, the effluents from the electroplating industry contain a variety of harmful compounds, including solvents, cleaning products, and heavy metals [2]. When released into the environment untreated, metals such as cadmium [Cd (II)], copper [Cu(II)], iron [Fe(II)], nickel [Ni(II)] and lead [Pb(II)] are particularly hazardous to human health even at low concentrations since they are toxic, highly mobile, and non-biodegradable [3,4]. For instance, Cd(II) is extremely harmful to human bone, kidneys, lungs, and is also carcinogenic [5,6]. Chronic conditions like liver and brain damage, irritability, sleeplessness, nausea, and diarrhoea can be caused by an excessive amount of Cu(II) accumulating in the body [7]. According to reports, wastewater with an excess of Fe(II) is carcinogenic, damages the intestinal tract, and irritates the respiratory system [8]. In addition,

* Corresponding author at: Department of Chemical Engineering, Chukwuemeka Odumegwu Ojukwu University, P.M.B 02, Uli Campus, Anambra State, Nigeria.
E-mail addresses: egbosiubachinedu@gmail.com, ct.egbosiuba@coou.edu.ng (T.C. Egbosiuba).

https://doi.org/10.1016/j.jece.2022.109180
Received 17 August 2022; Received in revised form 19 November 2022; Accepted 16 December 2022
Available online 22 December 2022

asthma, dermatitis, lung fibrosis, headaches, liver damage, brain haemorrhage, cardiac arrest, and carcinogenicity are all severe outcomes of prolonged exposure to nickel [9]. Also, Pb(II) has been associated with neurological diseases, cancer, anorexia, plumbism, anaemia, damage to the kidney, and impairment of the brain [10]. Given these challenges, there is an increasing global demand for the treatment of wastewater. To achieve this, World Health Organization (WHO) have recommended the allowable concentrations of 0.01, 1.0, 0.5, 0.07 and 0.1 mg/L for Cd(II), Cu(II), Fe(II), Ni(II) and Pb(II) ions in drinking water [11].

Numerous treatment technologies, including photocatalysis [12], membrane processes [13], coagulation/flocculation [14], reverse osmosis [15], advanced oxidation [16], electrochemical [17], and adsorption [18], have been used extensively in the treatment of heavy metals in water environments. Among them, adsorption is one of the most appealing treatment options because of its low-cost, adaptability, simplicity of use, low production of harmful by-products, and reusability of adsorbents [19,20]. For the treatment of wastewaters containing heavy metals, scientists have created a range of adsorbents recently. The majority of adsorbents, however, have a very limited adsorption capacity, and the effectiveness of their adsorption in severely acidic conditions was assessed. For the treatment of wastewaters containing heavy metals, researchers have recently created a range of adsorbents such as agricultural waste [21], biochar [22], activated carbon [23], zeolites [24,25], chitosan [26], carbon nanotubes (CNTs) [27] and graphene oxides [28]. However, most of the adsorbents such as biochar, activated carbon, zeolites and chitosan have a very limited adsorption capacity, instability challenges at low solution pH and complex regeneration that limits their practical application. In contrast, carbon nanotubes (CNTs) have been reported to have a good surface area, efficient recyclability and high stability under low solution pH, therefore presenting an excellent potential for practical application in wastewater treatment [29,30]. Although the adsorption capacity of pristine CNTs is relatively low and the adsorption rates slow due to the lack of well-developed binding sites for the adsorption process.

To enhance the surface properties of CNTs, several strategies have been employed for the purification and functionalization using oxidation, acid treatment, metal oxyhydroxide, metal nanoparticles, polyamine and incorporation of different materials [31]. Among these, acid treatment and incorporation of different materials to improve the functional groups have been employed to enhance metal ions adsorption capacities due to super electrostatic attraction and surface complexation between the functional groups and the metal ions. For instance, when modified with compounds which have the desired functionalities, CNTs have been found to have significant improvements in high adsorption capacity [32]. Particularly, CNTs have been used to remove various heavy metals from simulated and industrial wastewater [33–36]. To the best of our understanding, this study reports for the first time the treatment and functionalization of CNTs for the comparative adsorption of Ni(II), Fe(II), Cu(II), Cd(II), and Pb(II) from electroplating industrial wastewater.

In this study, carbon nanotubes were prepared using a chemical vapour deposition (CVD) technique. A high-performance acid-treated CNTs (TR-CNTs) and *p*-Nitrobenzoic acid functionalized CNTs (PN@TR-CNTs) were prepared by ultrasonication. The prepared CNTs, TR-CNTs and PN@TR-CNTs were characterized using x-ray diffraction (XRD), Fourier transform infrared spectroscopy (FTIR), high-resolution scanning electron microscopy (HRSEM), high-resolution transmission electron microscopy (HRTEM), energy dispersive x-ray (EDX) and Brunauer–Emmett–Teller (BET) analytical techniques. Overall, the comparative adsorption performance of the CNTs, TR-CNTs and PN@TR-CNTs was carried out. The effect of solution pH, nanoadsorbent dosage, contact time and temperature on the adsorption of Ni(II), Fe(II), Cu(II), Cd(II), and Pb(II) was investigated. The experimental data were fitted to the isotherm and kinetic models, while the thermodynamic parameters were also determined.

2. Materials and methods

2.1. Materials

All the chemicals utilized in this research were of analytical grade and obtained from Sigma Aldrich. The chemicals used in this study are cadmium sulphate ($CdSO_4$), copper (II) sulphate pentahydrate ($CuSO_4.5H_2O$), iron (II) sulphate heptahydrate ($FeSO_40.7\ H_2O$), nickel (II) sulphate hexahydrate ($NiSO_4.6H_2O$), lead (II) sulphate ($PbSO_4$), sodium hydroxide (NaOH), hydrochloric acid (HCl), trioxonitrate (V) acid (HNO_3), polyethylene glycol (PEG) and *p*-Nitrobenzoic acid with a purity range of 95.5–99.9%. The liquid nitrogen, nitrogen gases, acetylene, and argon gas were procured from the British Oxygen Company, Nigeria. Distilled water and deionized water were used for the solution preparations.

2.2. Fabrication of CNTs

The fabrication of CNTs involves two stages, the preparation of catalysts and the synthesis of CNTs. In the first stage, the preparation of bimetallic Fe-Ni catalyst assisted on kaolin support was achieved using the wet impregnation method reported elsewhere [37]. The bimetallic catalyst (Fe-Ni/kaolin) was synthesized by measuring 3.64 g of $FeSO_4.7H_2O$ and 5.05 g of $NiSO_4.6H_2O$ into a 200 mL beaker containing 10 g of kaolin. Afterwards, 50 mL of distilled water was added to the mixture and stirred steadily at 250 rpm on a magnetic stirrer for 30 min. Then, the sample was oven dried 110 °C for 16 h and ground using a mortar and a pestle. The ground samples were thereafter calcinated using a muffle furnace at 400 °C for 10 h. The sample was allowed to cool to room temperature, sieved through a 150 μm mesh size and stored in an airtight container labelled Fe-Ni/kaolin catalyst.

To synthesize CNTs, 1.0 g of Fe-Ni/kaolin catalyst was weighed into a quartz crucible and placed inside a chemical vapour deposition (CVD) furnace chamber. The argon gas flow rate was kept constant at 100 mL/min until the desired reaction temperature of 800 °C was attained. Thereafter, the acetylene gas flow rate was set at 250 mL/min and the argon gas flow rate increased to 300 mL/min until a reaction time of 60 min. In the end, the furnace was cooled to room temperature, while the weight of the produced CNTs was weighed and recorded as reported previously [37].

2.3. Purification and functionalization of CNTs

The synthesized CNTs were treated to remove catalyst impurities and other amorphous carbon. Particularly, 20 mL of HNO_3 and 60 mL of HCl (v/v 1:3) were mixed before the addition of 20 g of the synthesized CNTs. The mixture was stirred and sonicated at 40 °C for 90 min using ultrasonic bath to remove impurities and introduce an oxygen group to the CNTs surface. Thereafter, the mixture was steadily washed with deionized water and filtered using Whatman No. 42 filter paper until pH 7 was achieved. The obtained residue was dried in the oven at 110 °C for 12 h and stored in a sample bottle labelled TR-CNTs.

Furthermore, the TR-CNTs were functionalized by adding PEG (20.50 g, 512.50 mmol) and *p*-Nitrobenzoic acid (10.0 g, 60 mmol) to a 20 g of TR-CNTs contained in a 250 mL conical flask. Thereafter, the sample was placed in a sonication bath at 40 °C for 1 h for effective reaction with the surface structures of TR-CNTs. Afterwards, the obtained product was separated by centrifugation before the oven drying at 110 °C for 12 h. The obtained functionalized CNTs were stored in a safe container and labelled PN@TR-CNTs.

2.4. Characterisation of materials

The obtained CNTs, TR-CNTs and PN@TR-CNTs were characterised using X-ray diffraction (XRD), Fourier transform infrared spectroscopy (FTIR), high-resolution scanning microscopy (HRSEM), High-Resolution

transmission electron microscopy (HRTEM) and Brunauer Emmett Teller (BET) methods. The X-ray diffraction analysis was investigated on the samples using a Buker AXS D8 diffractometer. The diffractometer was equipped with a Cu Kα radiation source which functions in the range of 10–90°. The functional groups were performed using a Perkin Elmer spectrum FTIR spectrometer, USA. The spectra recorded for the samples are in the range of 4000–500 cm^{-1}. The morphology was examined by Zeiss Auriga HRSEM coupled with energy dispersive x-ray (EDX) and the microstructure was analysed by Zeiss Auriga HRTEM at an operating condition of 5 kV. The surface area and porosity were achieved using the Sorptometric 1990 Thermo Fisher Scientific Inc BET model.

2.5. Selected metal ions analysis

To investigate the adsorption effectiveness of the prepared nanoadsorbents, electroplating industry wastewater was collected from Minna, Niger State Nigeria. By using atomic adsorption spectrometry (AAS, PG 990, PG Instruments, UK), the residual metal ions concentration in the electroplating wastewater was determined as 18.40 mg/L for Cd(II), 20.39 mg/L for Cu(II), 19.52 mg/L for Fe(II), 23.70 mg/L for Ni (II) and 30.35 mg/L for Pb(II). To obtain an initial metal ion concentration of 0.1 g/L, each stock solution of the metal ions was prepared using 0.25 M of $CdSO_4$ (52.12 g), $CuSO_4.5H_2O$ (39.90 g), $FeSO_4.7H_2O$ (37.98 g), $NiSO_4.6H_2O$ (38.69 g) and $PbSO_4$ (75.82 g) in a litre of distilled water. In all the supernatant preparations, a water bath (SB25–12DT, Scientz) was utilized before filtration using Whatman No. 1 filter paper and the subsequent determination of the residual metal ions concentrations using the AAS method.

2.6. Batch adsorption study

Initially, the comparison of the removal efficiencies of CNTs, TR-CNTs and PN@TR-CNTs towards the selected Cd(II), Cu(II), Fe(II), Ni (II) and Pb(II) ions was conducted at constant pH (7), contact time (20 min), temperature (30 °C), initial metal concentration (0.1 g/L) and at different nanoadsorbent dosage (0.1, 0.2, 0.3, 0.4 and 0.5 g/L). Thereafter, TR-CNTs and PN@TR-CNTs with a higher adsorption capacity compared to CNTs were further applied to study their adsorption capacities towards Cd(II), Cu(II), Fe(II), Ni(II) and Pb(II) ions from electroplating wastewater in a batch adsorption experiment.

Overall, the batch adsorption study was examined at various pH (2, 3, 4, 5, 6, 7 and 8), contact times (10, 20, 30, 40, 50, 60 and 120 min), nanoadsorbent dosage (0.1, 0.2, 0.3, 0.4 and 0.5 g/L) and temperature (30, 35, 40, 45 and 50 °C). Briefly, 0.1 g/L each of TR-CNTs and PN@TR-CNTs were measured in a 250 cm^3 conical flask containing 50 mL of electroplating wastewater. The flask was corked and the mixture was shaken at different pH, contact times, nanoadsorbent dosage and temperatures using each of the TR-CNTs and PN@TR-CNTs. All adsorption tests were performed in triplicates and the average was recorded. At the end of the variations of pH, contact time, nanoadsorbent dosage and temperature, the solutions were filtered using Whatman No. 42 filter paper and the filtrate was analysed by atomic absorption spectrometry (AAS, PG 990, UK) to determine the residual concentrations of Cd(II), Cu (II), Fe(II), Ni(II) and Pb(II) ions.

The percentage removal (%) and adsorption capacity, q_e (mg/g) of the TR-CNTs and PN@TR-CNTs adsorbents were calculated using Eqs. (1) and (2) [38,39], respectively.

$$\text{Removal rate} = \frac{C_0 - C_e}{C_0} \times 100 \quad (1)$$

$$q_e = \frac{V(C_0 - C_e)}{W} \times 100 \quad (2)$$

where C_0 (mg/L) indicate the initial concentration of the metal in the wastewater, C_e (mg/L) refers to the residual concentration of the metal ions, W is the mass of the TR-CNTs and PN@TR-CNTs adsorbents (mg) and V is the volume of effluent (mL).

2.7. Reusability analysis

In this study, a regeneration study was carried out to evaluate the restoration of the retention capacity of TR-CNTs and PN@TR-CNTs towards the target pollutants. For this purpose, 0.1 M of NaOH and 0.1 M H_2SO_4 were used as a regeneration eluent to achieve metal ions release and practicability of reusability. Typically, 0.4 g/L of TR-CNTs and PN@TR-CNTs were introduced to a 0.1 g/L of the metal ions concentration and stirred vigorously at 50 °C for 1 h. The reusability effectiveness (R_e, %) investigation was repeated consecutively for six cycles, while the reusability capacity was calculated using Eq. (3) [40].

$$R_e(\%) = \frac{C_0 - C_e}{C_0} x100 \quad (3)$$

2.8. Statistical functions

Herein, the statistical experimental analysis was repeated in triplicate, while the isotherm, kinetic and thermodynamic constants were estimated at a 95% confidence level using Origin 2015 software. The evaluation of the experimental data fitness to the mathematical model was explored in this study by the determination coefficient (R^2) and the sum of square error (SSE) using the mathematical expressions presented in Eqs. (4) and (5) [41].

$$R^2 = 1 - \frac{\sum_{n=1}^{n}(q_{e.exp} - q_{e.cal})^2}{\sum_{n=1}^{n}(q_{e.exp} - q_{e.exp})^2} \quad (4)$$

$$SSE = \sum (q_{e,exp} - q_{e,cal})^2 \quad (5)$$

whereby $q_{e,exp}$ and $q_{e,cal}$ in (mg/g) refer to the experimental and calculated adsorption capacity at equilibrium, respectively.

3. Results and discussion

3.1. Characterization of materials

3.1.1. XRD analysis

The crystallographic structures of CNTs, TR-CNTs and PN@TR-CNTs were investigated by XRD patterns. As shown in Fig. 1a, three sharp diffraction patterns of CNTs were revealed at 2 Theta values of 26.52°, 44.50° and 51.60°. The determined XRD patterns showed correspondence to the graphite crystal planes of (002), (200) and (102), respectively [42]. The main diffraction patterns of the nanoadsorbents effectively matched the simulated peaks from the crystallographic information file [43,44]. The diffraction peak with the miller index (002) corresponds to hexagonal graphite and also referred to the spacing between graphite carbon la**yers.** The diffraction patterns of the nanoadsorbents clearly showed that the structure of the CNTs was significantly retained even after acid purification and functionalization using PEG and *p*-Nitrobenzoic acid. Also, another small peak identified at 74.75° on the CNTs, TR-CNTs and PN@TR-CNTs which may be attributed to the presence of carbon. However, the crystalline peaks identified on the TR-CNTs and PN@TR-CNTs at 67.91° may be linked to the acid treatment effect of the nanoadsorbents. Remarkably, diffraction patterns occurrence at 21.72°, 37.73°, 38.66° and 60.02° on the PN@TR-CNTs may be due to the functionality modifications of the crystalline structure by PEG and *p*-Nitrobenzoic acid. The determined average crystallite sizes of 16.96, 22.32 and 30.77 nm were obtained for CNTs, TR-CNTs and PN@TR-CNTs using the Debye-Scherrer equation [45].

3.1.2. FTIR analysis

The information on the characteristic functional groups of the CNTs,

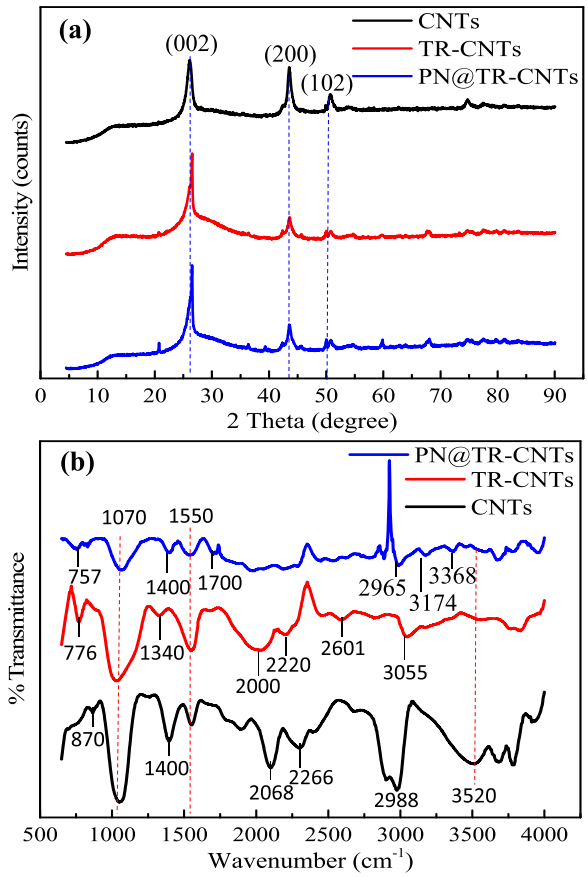

Fig. 1. (a) XRD diffraction patterns and (b) FTIR spectra of CNTs, TR-CNTs and PN@TR-CNTs.

TR-CNTS and PN@TR-CNTs were identified by FTIR spectra and the results are presented in Fig. 1b. As can be seen in Fig. 1b, there were remarkable differences between the occurrence of the peaks on CNTs, TR-CNTS and PN@TR-CNTs. According to the results, the characteristic peak at 870, 776 and 755 cm^{-1} for CNTs, TR-CNTS and PN@TR-CNTs were assigned to the C-H bending vibrations of the alkane and aromatic groups. Furthermore, the absorption peaks common to the nanoadsorbents were identified at 1070, 1550 and 3520 cm^{-1}, which were attributed to the alkoxy C-O, C═C stretch and O-H stretch due to alcohol. The C-H bending vibrations that occurred at 1400 cm^{-1} on the CNTs shifted to lower wavenumber (1340 cm^{-1}) after acid treatment on the TR-CNTs but reappeared with reduced intensity on the PN@TRCNTs. Particularly, the peak at 1700 cm^{-1} defined on the PN@TR-CNTs corresponds to the C═O stretching vibrations of the carboxylic acid that emanated from the free azobenzene dicarboxylic acid [46]. Above all, the absence of this peak on the CNTs and TR-CNTs indicates that PN@TR-CNTs were successfully prepared. The presence of other peaks vibrations on CNTs at 2068, 2266 and 2988 cm^{-1} were assigned to the stretching vibrations of C≡C, C≡N and C-H bonds. On the TR-CNTs, the presence of peaks at the wavenumber of 2000, 2220, 2601 and 3055 cm^{-1} were assigned to the C═O, C≡N, C-H and O-H groups due to the acid treatment. The vibrations at 2965, 3174 and 3368 cm^{-1} on the PN@TR-CNTs were attributed to C-H and O-H stretching bands attributed to the functional presence of PEG and *p*-Nitrobenzoic acid. These results proved successful synthesis of CNTs, acid purification of TR-CNTs and surface functionalization of the PN@TR-CNTs using PEG and *p*-Nitrobenzoic acid for enhanced carbonyl, carboxyl and hydroxyl functional groups towards the adsorptive removal of the metal ions from electroplating wastewater.

3.1.3. Morphological analysis

The HRSEM micrographs of the CNTs, TR-CNTS and PN@TR-CNTs shown in Fig. 2(a,b,c) provided the morphologies and network structures.

As shown in Fig. 2(a,b,c), the nanoadsorbents showed rough, spongy, non-uniform and agglomerated clusters of carbonaceous material on the networked tubular surface. It is evident in Fig. 2b that a rougher surface and larger diameter of TR-CNTs compared to CNTs in Fig. 2a, thereby leading to reduction in diameter uniformity. Remarkably, the surface of TR-CNTs is smoother due to acid functionalization, while the surface of PN@TR-CNTs (Fig. 2c) revealed a networked surface coverage by a thin layer and the associated diameter increment [47]. In Fig. 2b, the aligned smooth surface of TR-CNTs was attributed to the removal of impurities and amorphous carbon through the purification process. The HRSEM of PN@TR-CNTs presented in Fig. 2c indicated clear, aggregated and networked tubes of different diameters with the presence of whitish particles that showed successful incorporation of carboxylic functional groups on the networked surface matrix of the PN@TR-CNTs. The observed surface aggregation of the nanoadsorbents may be attributed to the rough surface adsorption of the tubular networks [44]. As can be seen after functionalization, the diameter of the CNTs obtained increased significantly due to the wrapping of the additional functional group such as C═O, C-O, O-H, C-N and C-H by the CNTs. In general, the diameters of the nanoadsorbents were evaluated in the range of 15–100 nm.

3.1.4. Microstructural analysis

Further investigation of the microstructure of CNTs, TR-CNTs and PN@TR-CNTs was conducted by HRTEM. The results of the corresponding microscopic image of the nanoadsorbents are shown in Fig. 2 (d,e,f). As can be seen in Fig. 2d, the presence of a dense black-coloured spot suggested the occurrence of amorphous carbon and residual particles from kaolin-supported catalysts. However, after acid treatment, the carbonaceous material and other impurities present on the surface of CNTs were significantly reduced (Fig. 2e). Above all, the functionalized PN@TR-CNTs revealed a dark spot due to the incorporated *p*-Nitrobenzoic acid encapsulated within the tubular structures of CNTs. Hence, it can be intuitively adjudicated that TR-CNTs modified *p*-Nitrobenzoic acid was successfully fabricated with an average particle size of 30.50 nm.

3.1.5. Elemental analysis

The EDS of the CNTs, TR-CNTs and PN@TR-CNTs showing the compositions of elements are depicted in Fig. S1(a,b,c) (Supplementary material). As can be seen in Fig. S1(a,b,c) the presence of the C, O, Al, Si. Fe and Ni are provided in percentage elemental composition. In all CNTs spectra, the amount of carbon was higher than other elements which confirms that graphite is the predominant component of the nanoadsorbent. Typically, the carbon content in CNTs (81.23%) increased to 84.55% and 94.18% after purification and functionalization. The occurrence of Al, Si, O, Fe and Ni in the CNTs was from kaolin support and Fe/Ni catalyst used for the CNTs synthesis (Fig. S1a). Also, the reduction in the percentage composition of the impurities was evident after purification (Fig. S1b) and functionalization (Fig. S1c). This suggests that purification and functionalization effectively removed impurities and enhanced surface functional moieties that are beneficial to the effectiveness of the nanoadsorbents in wastewater treatment. In addition, a sharp increase was demonstrated by the oxygen peak for CNTs, TR-CNTs and PN@TR-CNTs after purification and functionalization due to the acid treatment and incorporation of functional groups.

3.1.6. Surface properties analysis

The specific surface area, pore volume and pore size of the CNTs, TR-CNTs and PN@TR-CNTs were measured by the N_2 adsorption method. According to the results, 583.31 $m^2\ g^{-1}$, 0.2963 $cm^3\ g^{-1}$ and 16.83 nm were obtained as the surface area, pore volume and pore size of CNTs,

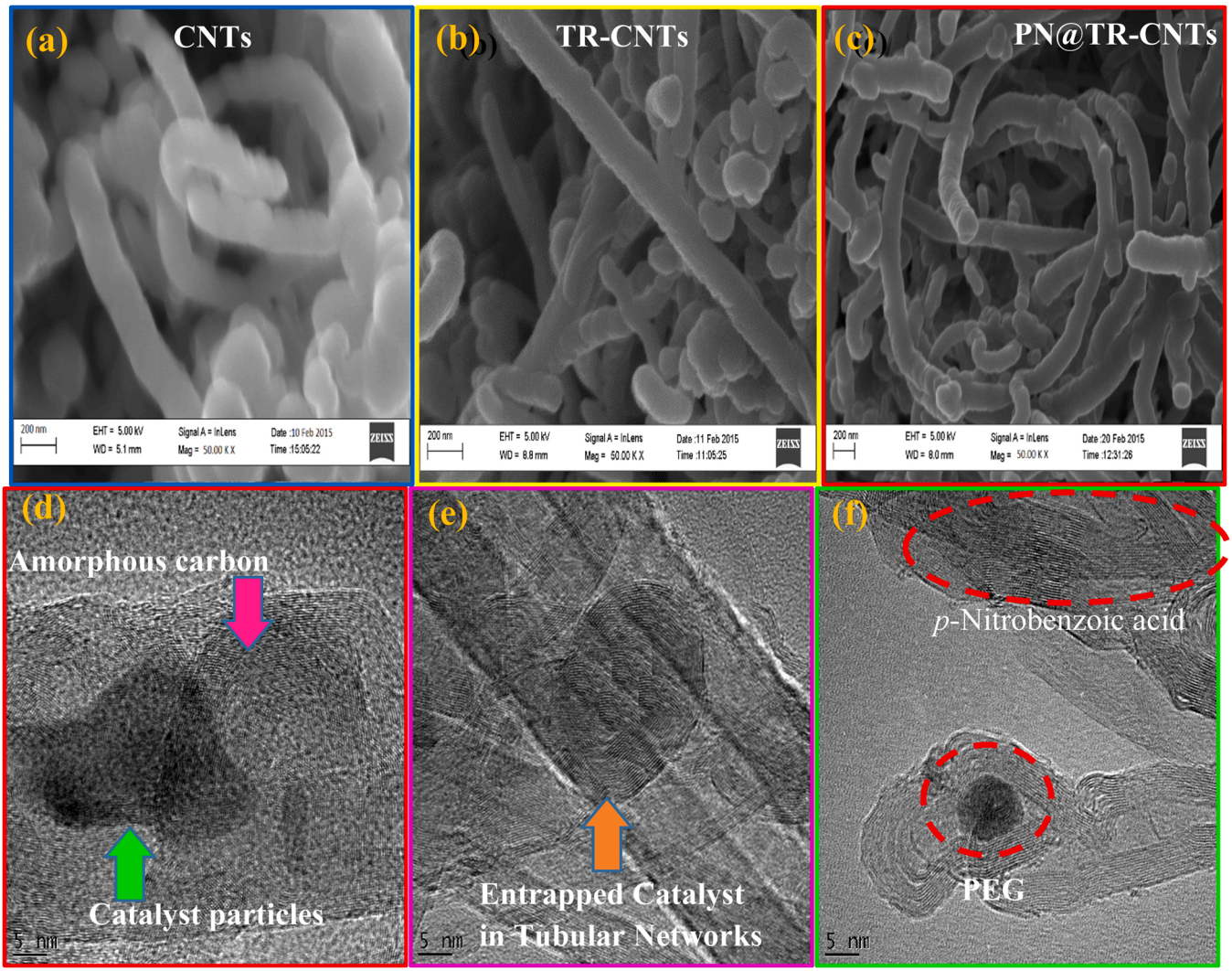

Fig. 2. HRSEM patterns of (a) CNTs; (b) TR-CNTs; (c) PN@TR-CNTs; HRTEM patterns of (d) CNTs; (e) TR-CNTs and (f) PN@TR-CNTs.

while TR-CNTs showed the surface area, pore volume and pore size of 781.88 $m^2\ g^{-1}$, 0.325 $cm^3\ g^{-1}$, 22.04 nm. The observed higher surface area of TR-CNTs over CNTs may be linked to successful the acid purification technique that removed amorphous carbon and unreacted metallic impurities, thereby opening both CNTs end caps and sidewalls [48,49]. Furthermore, the functionalized PN@TR-CNTs showed a surface area, pore volume and pore size of 970.81 $m^2\ g^{-1}$, 0.346 $cm^3\ g^{-1}$ and 31.21 nm. The observed increment in the surface properties of PN@TR-CNTs after functionalization may be attributed to the incorporation of additional functional groups into the networked tubular structure of CNTs. The surface properties of the nanoadsorbents followed the incremental trend of PN@TR-CNTs > TR-CNTs > CNTs. This indicates greater availability of interfacial area and active sites for the occurrence of nanoadsorbent/metal ions interaction that enhances the removal of metal ions from wastewater in PN@TR-CNTs CNTs compared to TR-CNTs and CNTs. Importantly too, the pore sizes of the nanoadsorbents were in the mesoporous range of 2–50 nm, thus signifying that the materials are mesoporous in nature. The results of the surface properties of CNTs, TR-CNTs and PN@TR-CNTs showed successful purification and functionalization of the nanoadsorbents, thereby corresponding with the XRD patterns, FTIR spectrum, HRSEM and HRTEM micrographs.

3.2. Performance comparison of the nanoadsorbents

Herein, CNTs, TR-CNTs and PN@TR-CNTs were all examined for the comparison of Cd(II), Cu(II), Fe(II), Ni(II) and Pb(II) removal performance. The adsorption capacities of Cd(II), Cu(II), Fe(II), Ni(II) and Pb (II) for CNTs, TR-CNTs and PN@TR-CNTs are shown in Fig. 3(a,b,c) at various nanoadsorbent mass. From Fig. 3c, it is evident that PN@TR-CNTs recorded highest adsorption capacity of 160.08 mg/g for Cd(II), 201.86 mg/g for Cu(II), 170.60 mg/g for Fe(II), 226.00 mg/g for Ni(II) and 250.39 mg/g for Pb(II) compared to Cd(II) (142.71 mg/g), Cu(II) (164.99 mg/g), Fe(II) (152.67 mg/g), Ni(II) (198.89 mg/g), Pb(II) (224.59 mg/g) and Cd(II) (100.39 mg/g), Cu(II) (150.89 mg/g), Fe(II) (125.34 mg/g), Ni(II) (179.93 mg/g), Pb(II) (198.49 mg/g) obtained for TR-CNTs (Fig. 3b) and CNTs (Fig. 3a) respectively at adsorbent mass of 0.5 g/L. According to this finding, PN@TR-CNTs were more effective in the removal of the metal ions from electroplating industry wastewater, followed by TR-CNTs and CNTs. The remarkable greater specific surface area of PN@TR-CNTs compared to TR-CNTs and CNTs may be ascribed to the higher effectiveness in the removal of the metal ions. Additionally, the introduction of further carbonyl, carboxyl and hydroxyl functional groups through treatment and functionalization in the case of TR-CNTs and PN@TR-CNTs may be attributed to the observed increased reactivity towards the metal ions and their eventual elimination from the wastewater [50]. The increased number of active sites accessible for adsorption is connected to the observed enhanced metal ions adsorption

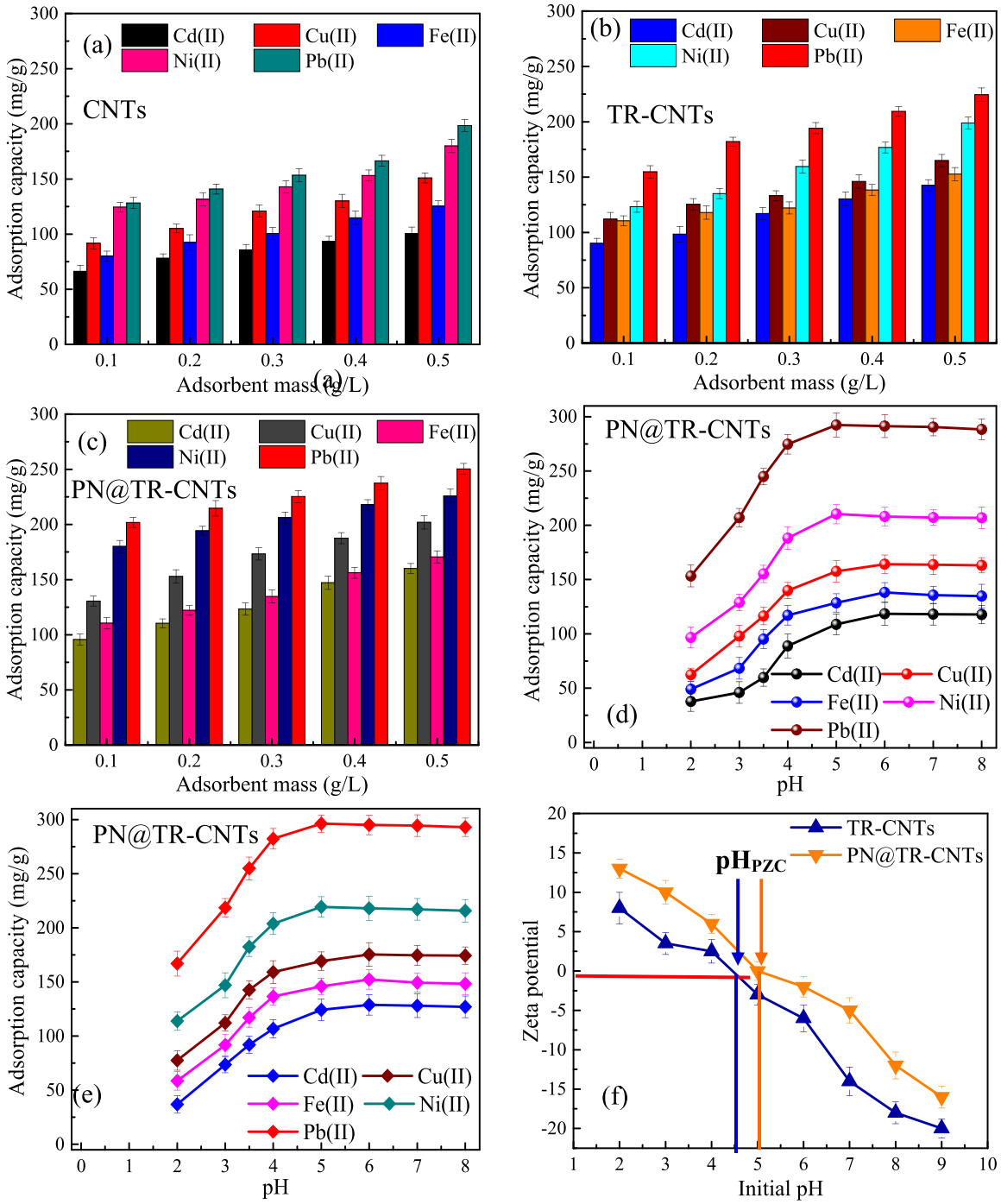

Fig. 3. Comparison adsorption performance of Cd(II), Cu(II), Fe(II), Ni(II) and Pb(II) using (a) CNTs; (b) TR-CNTs; (c) PN@TR-CNTs at various nanoadsorbent dosage (pH of 5, contact time of 30 min and temperature of 303 K). The effect of pH on the adsorption of Cd(II), Cu(II), Fe(II), Ni(II) and Pb(II) using (d) TR-CNTs; (e) PN@TR-CNTS and (f) zeta potential of TR-CNTs and PN@TR-CNTs.

capacity with the increasing nanoadsorbent mass. Further adsorption studies for the metal ions removal from wastewater were carried out using TR-CNTs and PN@TR-CNTs due to their higher adsorption capacities compared to the pristine CNTs.

3.3. Adsorption studies

3.3.1. Effect of pH

Overall, one of the key factors significantly impacting the adsorption process is the initial pH of the metal ions solution. This is because it affects interactions between the surface species of the nanoadsorbent and the adsorbate ions as well as the charged species that will form at the surface of the nanoadsorbent. Fig. 3(d,e) illustrates how initial solution pH affects TR-CNTs and PN@TR-CNTs ability to remove Cd(II), Cu(II), Fe(II), Ni(II) and Pb(II) from wastewater. The Cd(II), Cu(II), Fe(II), Ni (II), and Pb(II) adsorption capacity of TR-CNTs and PN@TR-CNTs was significantly decreased within the pH range of 2–4, whereas a considerable increase in adsorption capacity was achieved within the range of pH 4–6. It is evident from the results that the maximum adsorption capacities of 118.50, 164.14 and 138.20 mg/g for Cd(II), Cu(II) and Fe(II) were obtained at pH 6 using TR-CNTs, while 128.80, 175.35 and 152.27 mg/g of the metal ions were achieved at the same pH. In

contrast, the maximum adsorption capacities for Ni(II) and Pb(II) ions were obtained as 210.38 and 292.36 mg/g using TR-CNTs, while that of PN@TR-CNTs are 219.27 and 296.28 mg/g, respectively when the pH was 5.

The pH_{PZC} of TR-CNTs and PN@TR-CNTs was determined to be 4.5 and 5, as shown in Fig. 3f, indicating that the surface of the nano-adsorbents exhibits electropositivity (protonated) at pH levels below 4.5 and 5, while being negatively charged (deprotonated) at pH levels above 4.5 and 5. Due to electrostatic repulsion ascribed to interactive competitiveness between protons (H^+) and metal ions, positive metal ions are unfavourable for interacting with the positively charged surface of nanoadsorbents at $pH < pH_{PZC}$ [10]. Nevertheless, this unfavourable effect gradually decreases as pH increases, leading to enhanced adsorption. Therefore, at higher pH levels ($pH > 4.5/5$) the negatively charged (deprotonated) surface of the adsorbent favours greater metal ions removal efficiency. The trend of this result demonstrates that the adsorption process is significantly influenced by repulsive electrostatic forces [51]. At pH levels above 5 and 6, the potential for Ni(II), Pb(II),

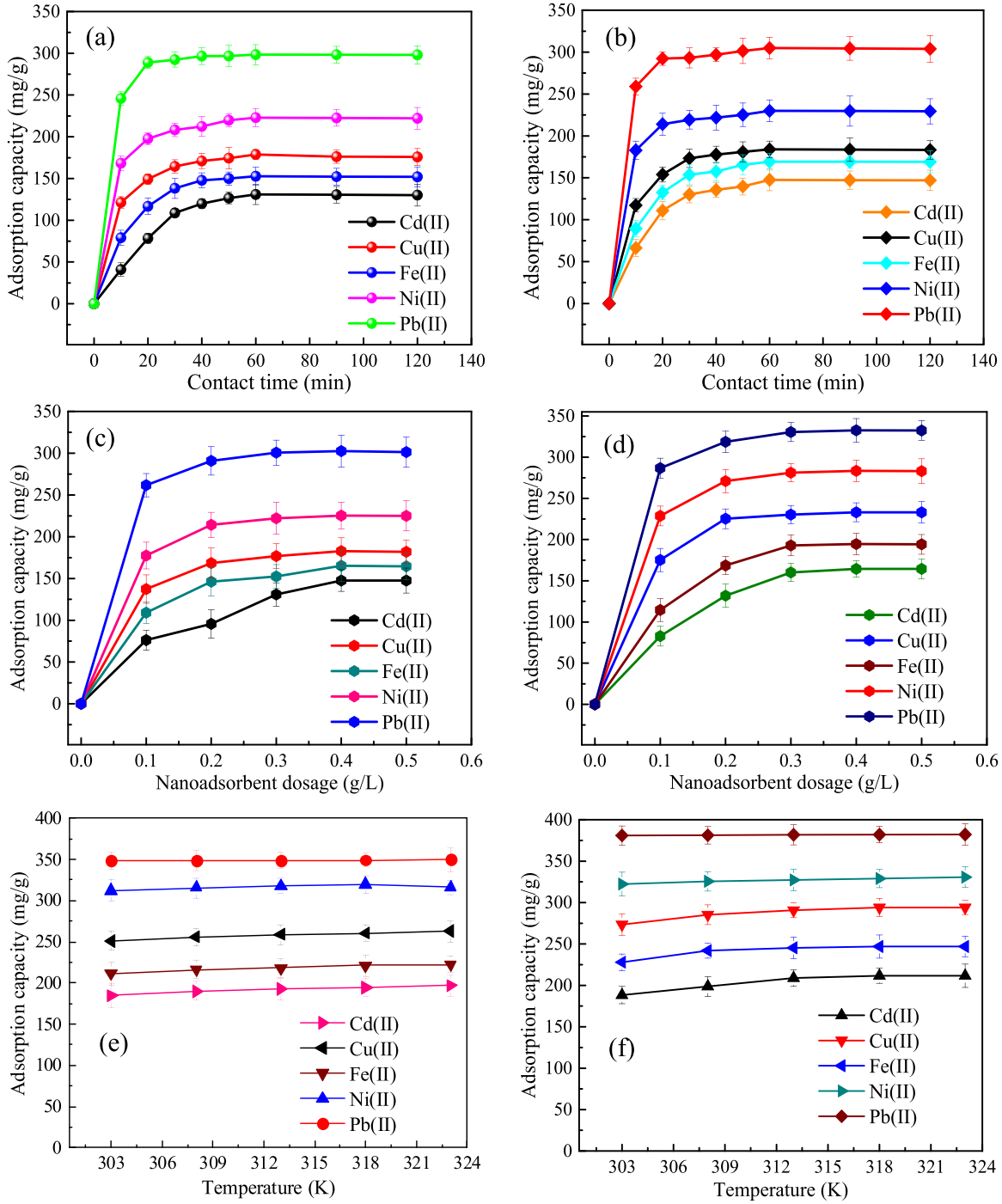

Fig. 4. The effect of nanoadsorbent dosage on the adsorption of Cd(II), Cu(II), Fe(II), Ni(II) and Pb(II) using (a) TR-CNTs and (b) PN@TR-CNTS (conditions: pH of 5 (Ni(II) and Pb(II)) and 6 (Cd(II), Cu(II) and Fe(II)), contact time of 30 min and temperature of 303 K); the effect of contact time on the adsorption of Cd(II), Cu(II), Fe (II), Ni(II) and Pb(II) using (c) TR-CNTs and (d) PN@TR-CNTS (conditions: pH of 5 (Ni(II) and Pb(II)) and 6 (Cd(II), Cu(II) and Fe(II)), nanoadsorbent dosage of 0.4 g/L and temperature of 303 K); the effect of temperature on the adsorption of Cd(II), Cu(II), Fe(II), Ni(II) and Pb(II) using (e) TR-CNTs and (f) PN@TR-CNTS (conditions: pH of 5 (Ni(II) and Pb(II)) and 6 (Cd(II), Cu(II) and Fe(II)), nanoadsorbent dosage of 0.4 g/L and contact time of 60 min).

Cd(II), Cu(II) and Fe(II) oxyhydroxide precipitation on the surface of the nanoadsorbents may have caused a minor reduction in removal effectiveness. This finding confirms that the optimal removal of Ni(II) and Pb (II) by TR-CNTs and PN@TR-CNTs, was accomplished at pH 5, while that of Cd(II), Cu(II), and Fe(II), was better removed at pH 6.

3.3.2. Effect of contact time

In this study, the effect of contact time on the adsorption capacity of Cd(II), Cu(II), Fe(II), Ni(II) and Pb(II) using TR-CNTs and PN@TR-CNTs was varied for 10, 20, 30, 40, 50, 60, 90 and 120 min at a constant pH (5 (for Ni(II) and Pb(II)) and 6 (for Cd(II), Cu(II) and Fe(II)), adsorbent dosage (0.4 g/L) and temperature (303 K). The result presented in Fig. 4 (a,b) revealed a rapid removal of the metal ions within the first 30 min which was attributed to the availability of a large number of binding sites at this period. Particularly, the defensive force between the free metal ions in the adsorbate solution and the adsorbed metal ions on the surface of the TR-CNTs/PN@TR-CNTs may decline the availability of the binding sites on the nanoadsorbents [51]. The adsorption of the metal ions increased gradually after 30 min until equilibrium saturation was attained at 60 min for both TR-CNTs and PN@TR-CNTs. Notably, the TR-CNTs adsorption capacity for Cd(II), Cu(II), Fe(II), Ni(II) and Pb (II) at the saturation stage were 130.88, 178.84, 152.67, 222.91 and 298.40 mg/g. On the other hand, a higher adsorption capacity of 147.57, 183.88, 169.25, 229.97 and 304.92 mg/g were achieved for Cd (II), Cu(II), Fe(II), Ni(II) and Pb(II) using PN@TR-CNTs after 60 min. Beyond the contact time of 60 min, no observable increment was evident for all the metal ions using both nanoadsorbents.

It is evident in this study that PN@TR-CNTs removed all metal ions better than TR-CNTs at different contact times and may be ascribed to the abundant carboxyl, carbonyl and hydroxyl functional groups incorporated onto the nanoadsorbent through functionalization. Also, the removal of Pb(II) and Ni(II) was higher compared to Cu(II), Fe(II) and Cd(II) at each experimental condition. Particularly, the removal differences of these metal ions may be due to their variations in electronegativity and ionic radius [52]. The electronegativity of the metal ions in this study is 1.69 for Cd(II), 1.90 for Cu(II), 1.83 for Fe(II), 1.91 for Ni(II) and 2.33 for Pb(II), while their ionic radius is 0.78 Å for Cd(II), 0.73 Å for Cu(II), 0.64 Å for Fe(II), 0.55 Å for Ni(II0 and 0.98 Å for Pb (II) [53–55]. Metal ions with greater electronegativity levels and smaller ionic radii adsorb more quickly than those with lower electronegativity levels and larger ionic radii [56]. The adsorption trend of the nanoadsorbents towards the metal ions followed the electronegativity levels, whereby the adsorption capacity followed the trend Pb(II)>Ni(II)>Cu (II)>Fe(II)>Cd(II). It is evident that higher electronegativity Pb(II), Ni (II), and Cu(II) ions had better access to the pores of nanoadsorbents and increased removal efficiency than Fe(II) and Cd(II), respectively. The removal of the metal ions was, however, favoured by a smaller ionic radius, except for Cu(II), which was eliminated before Fe(II).

3.3.3. Effect of nanoadsorbent dosage

The influence of nanoadsorbent dosage of TR-CNTs and PN@TR-CNTs on the removal of Cd(II), Cu(II), Fe(II), Ni(II) and Pb(II) at a temperature of 30 ℃ is depicted in Fig. 4(a,b). From the experimental results in Fig. 4c, it can be concluded that Cd(II), Cu(II), Fe(II), Ni(II) and Pb(II) adsorption capacity increased from 76.21 to 147.60 mg/g, 137.43–182.82 mg/g, 109.15–165.30 mg/g, 177.44–226.33 mg/g and 231.74–292.85 mg/g with respect to increment in TR-CNTs nanoadsorbent dosage from 0.1 to 0.4 g/L at the initial metal ions concentrations of 50 mg/L, contact time of and pH of 5 (Ni(II), Pb(II)) and 6 (Cd (II), Cu(II), Fe(II)). Similarly, it can be seen in Fig. 4d that the adsorption capacities of Cd(II), Cu(II), Fe(II), Ni(II) and Pb(II) increased from 82.84 to 164.44 mg/g, 175.24–233.12 mg/g, 114–194.24 mg/g, 228.72–283.47 mg/g and 286.75–332.43 mg/g as the PN@TR-CNTs nanoadsorbent dosage was increased from 0.1 to 0.4 g/L. Noticeably, a further increase in both nanoadsorbent dosages to 0.5 g/L resulted in a minimal decline in the adsorption capacity of the metal ions. The removal efficiency increases with the increase in nanoadsorbent dosage due to a high number of absorption sites [57]. However, further increase beyond a certain level saturated the available adsorption sites, reducing the adsorption [58]. Similar results were observed to remove metal ions using functionalized chitosan and spent lithium-ion battery as adsorbents [10,59]. The theory of available adsorption sites explained the results of the adsorption. The higher surface area of PN@TR-CNTs over TR-CNTs provides ample adsorption sites for increased adsorption efficiency toward the metal ions removal.

3.3.4. Effect of temperature

In this study, the influence of temperatures (303, 308, 313, 318 and 323 K) on the adsorption capacity of TR-CNTs and PN@TR-CNTs for Cd (II), Cu(II), Fe(II), Cd(II) and Pb(II) adsorption is displayed in Fig. 4(e,f). According to the results, an increase in metal ions adsorption was observed from 184.50 to 196.65 mg/g for Cd(II), 251.05–262.64 mg/g for Cu(II), 211.70–222.48 mg/g for Fe(II), 312.05–316.27 mg/g for Ni (II) and from 348.88 to 349.37 mg/g for Pb(II) with solution temperature increase from 303 to 323 K using TR-CNTs. Similarly, an increasing trend in the adsorption capacity of PN@TR-CNTs for Cd(II), Cu(II), Fe (II), Cd(II) and Pb(II) adsorption was observed to increase from 188.28 to 211.60 mg/g, 273.46–294.05 mg/g, 227.91–246.95 mg/g, 322.21–330.66 mg/g and 380.98–382.12 mg/g, respectively, with increasing solution temperature from 303 to 323 K. The increasing trend of the adsorption capacity with temperature elevation indicates that the removal of the metal ions on both nanoadsorbents was endothermic and spontaneous due to enhanced interaction between the metal ions and the nano adsorbent that increased the kinetic energy and elevated mobility of the metal ions for increased diffusion to the surface of TR-CNTs/PN@TR-CNTs [57,60]. Additionally, more active sites and pores were activated on the surfaces of TR-CNTs and PN@TR-CNTs at higher temperatures, which may be ascribed to the possible surface impurities removal with increasing temperature [46]. The obtained result is consistent with earlier findings on the adsorption of Cd(II), Cu(II), Fe(II), Ni(II), and Pb(II) onto various adsorbent materials [61–65].

3.4. Isotherm studies

The adsorption isotherms can show how the adsorbed Cd(II), Cu(II), Fe(II), Ni(II), and Pb(II) are distributed across the solid and liquid phases on the achievement of equilibrium adsorption state. Four adsorption isotherm models were used in this study to fit the experiment results, including Langmuir, Freundlich, Redlich-Peterson, and Sips (Langmuir-Freundlich). The four model equations were presented in Table 1, whereas Fig. 5 showed the results of the nonlinear regression fitting and Table 1 identified the pertinent parameters. As can be seen from the results, all of the isotherm models provided a good fit to the experimental data of the metal ions. However, the comparison for the best fit was based on the sum of square errors (SSE) and coefficient of determination (R^2) presented in Table 1. For a more thorough assessment of the models goodness of fit, the error functions for the analyzed isotherm models were generated and the findings are shown in Table 1. It had been reported previously that error analysis of the nonlinear forms of the models provided a more accurate way to calculate the isotherm parameters [66]. The Redlich-Peterson model fits the experimental data more closely than other models when comparing the four isotherm models, because of their greater R^2 and lower SSE values. For Redlich-Peterson and Sips models, it suggested that metal ions removal was not ideal monolayer adsorption, but a combination of physisorption and chemisorption processes that demonstrate the heterogeneity of Cd (II), Cu(II), Fe(II), Ni(II) and Pb(II) adsorption on the surface of TR-CNTs and PN@TR-CNTs. Overall, the obtained trend of the goodness of fit is Redlich-Peterson > Sips > Langmuir > Freundlich.

Table 1
Adsorption isotherm constants for the adsorption of metal ions by TR-CNTs and PN@TR-CNTs.

Model/Mathematical Expression	Adsorbent	Parameters	Cd (II)	Cu (II)	Fe (II)	Ni (II)	Pb (II)
Langmuir $q_e = \frac{q_m K_L C_e}{1 + K_L C_e}$	TR-CNTs	**q_m(mg/g)**	170.911	202.604	191.571	227.536	319.230
		K_L (L/mg)	5.023	22.088	14.017	26.942	47.033
		R^2	0.984	0.985	0.986	0.989	0.990
		SSE	0.052	0.064	0.047	0.051	0.085
	PN@TR-CNTs	**q_m(mg/g)**	224.072	261.530	243.070	306.499	351.251
		K_L (L/mg)	6.740	22.925	10.114	31.450	46.023
		R^2	0.988	0.97	0.985	0.989	0.993
		SSE	0.055	0.080	0.085	0.070	0.092
Freundlich $q_e = K_F C_e^{\frac{1}{n}}$	TR-CNTs	**n_F**	2.252	5.873	4.170	6.952	9.981
		K_F (mg/g)/(L/mg)$^{1/n}$	210.793	212.291	201.942	257.990	329.070
		R^2	0.981	0.984	0.982	0.985	0.987
		SSE	1.324	1.504	1.217	1.032	1.170
	PN@TR-CNTs	**n_F**	2.633	6.261	3.392	7.950	10.934
		K_F (mg/g)/(L/mg)$^{1/n}$	229.880	272.011	253.891	318.063	366.012
		R^2	0.983	0.985	0.984	0.987	0.986
		SSE	1.022	1.240	1.433	1.701	1.650
Redlich-Peterson $q_e = \frac{q_{RP} K_{RP} C_e}{1 + (K_{RP} C_e)^n}$	TR-CNTs	q_{RP}	163.091	197.990	160.432	270.223	314.360
		K_{RP} (L/mg)	47.913	30.890	32.524	21.990	14.512
		n	0.812	0.443	0.482	0.402	0.233
		R^2	0.992	0.995	0.993	0.996	0.997
		SSE	0.003	0.005	0.002	0.001	0.002
	PN@TR-CNTs	q_{RP}	129.892	209.341	183.604	260.392	357.160
		K_{RP}(L/mg)	25.474	15.220	20.302	13.174	9.754
		n	0.592	0.582	0.651	0.520	0.381
		R^2	0.991	0.997	0.995	0.998	0.999
		SSE	0.004	0.006	0.001	0.008	0.005
Sips $q_e = \frac{q_S (K_S C_e)^n}{1 + (K_S C_e)^n}$	TR-CNTs	**qs (mg/mg)**	182.080	218.974	200.492	219.511	328.042
		Ks (L/mg)	0.140	0.161	0.242	0.141	0.093
		n	1.040	1.682	1.451	1.380	1.032
		R^2	0.989	0.991	0.988	0.993	0.995
		SSE	0.041	0.032	0.025	0.045	0.013
	PN@TR-CNTs	**qs(mg/mg)**	228.46	270.99	239.48	317.05	361.00
		Ks (L/mg)	0.381	0.160	0.301	0.132	0.090
		n	1.410	1.022	14.412	1.023	1.004
		R^2	0.990	0.995	0.992	0.995	0.996
		SSE	0.017	0.011	0.020	0.018	0.010

where qe (mg/g) is the amount of metal ions adsorbed at equilibrium; Ce (mg/L) is the metal ions concentration at equilibrium; KL (L/g) is the Langmuir constant; qm (mg/g is the Langmuir adsorption capacity; KF (mg/g)/(mg/L)n is the Freundlich constant; n (dimensionless) is the exponential representation of the model; KS (L/mg) is the Sips constant; qS (mg/g) is the Sips adsorption capacity; KRP (L/mg) is the Redlich–Peterson constant and qRP (mg/g) is the Redlich–Peterson adsorption capacity.

3.5. Kinetic studies

In the kinetics study, mathematical models were proposed for the description of adsorption classification into diffusion and reaction models. In adsorption diffusion models, the three basic steps followed are external diffusion, intraparticle (internal) diffusion and the exchange process between the binding sites of the nanoadsorbent and the metal ions [66]. Then again, the adsorption reaction models involve the unconsidered chemical reactions in the modelling of the adsorption process. The evaluated kinetic models in this study include pseudo-first order, pseudo-second order, Elovich and intraparticle diffusion (IPD) models as mathematically represented in Table 2. The fitting results of the adsorption kinetic experimental data to the kinetic models are shown in Fig. 6.

Accordingly, the adsorption of Cd(II), Cu(II), Fe(II), Ni(II) and Pb(II) ions onto the TR-CNTs and PN@TR-CNTs were time-dependent and provides possible information on the adsorption mechanism of the metal ions. The evaluated kinetic adsorption parameters and error functions are presented in Table 2. As can be seen from the presented parameters, the pseudo-second order kinetic model suitably fitted the experimental data better than the pseudo-first order, Elovich and intraparticle diffusion models. The trend of the kinetic results is an indication that the metal ions adsorption by TR-CNTs and PN@TR-CNTs were dominated by chemisorption due to chemical bonding and electrostatic interaction between the Cd(II)/Cu(II)/Fe(II)/Ni(II)/Pb(II) ions and the TR-CNTs/PN@TR-CNTs [67]. Based on the assumption of the Elovich model that the adsorbent surface is energetic and heterogenous, the interactions and desorption between the adsorbed metal ions do not influence the adsorption kinetics at low coverage of the surface. Particularly, the obtained higher values of the initial adsorption rate (α) compared to the desorption constant (β) is an indication of adsorption interaction effectiveness between the nanoadsorbents and the metal ions.

3.6. Thermodynamic studies

To determine the viability, spontaneity, unpredictability, and endothermic/exothermic nature of the removal process, thermodynamics analyses of Cd(II), Cu(II), Fe(II), Cd(II), and Pb(II) adsorption onto TR-CNTs and PN@TR-CNTs were performed. By examining the adsorptive nature of Cd(II), Cu(II), Fe(II), Cd(II), and Pb (1I) onto TR-CNTs and PN@TR-CNTs using Eqs. (6), (7) and (8) [68–70], the thermodynamic parameters, such as the adsorption systems change in Gibbs free energy (ΔG°, kJ/mol), adsorption systems change in enthalpy (ΔH°, kJ/mol), and adsorption systems change in entropy (ΔS°, kJ/mol) were determined.

$$\Delta G^\circ = -RT\ln k_d \tag{6}$$

$$k_d = \frac{q_e}{C_e} \tag{7}$$

$$\ln k_d = \frac{\Delta S^\circ}{R} - \frac{\Delta H^\circ}{RT} \tag{8}$$

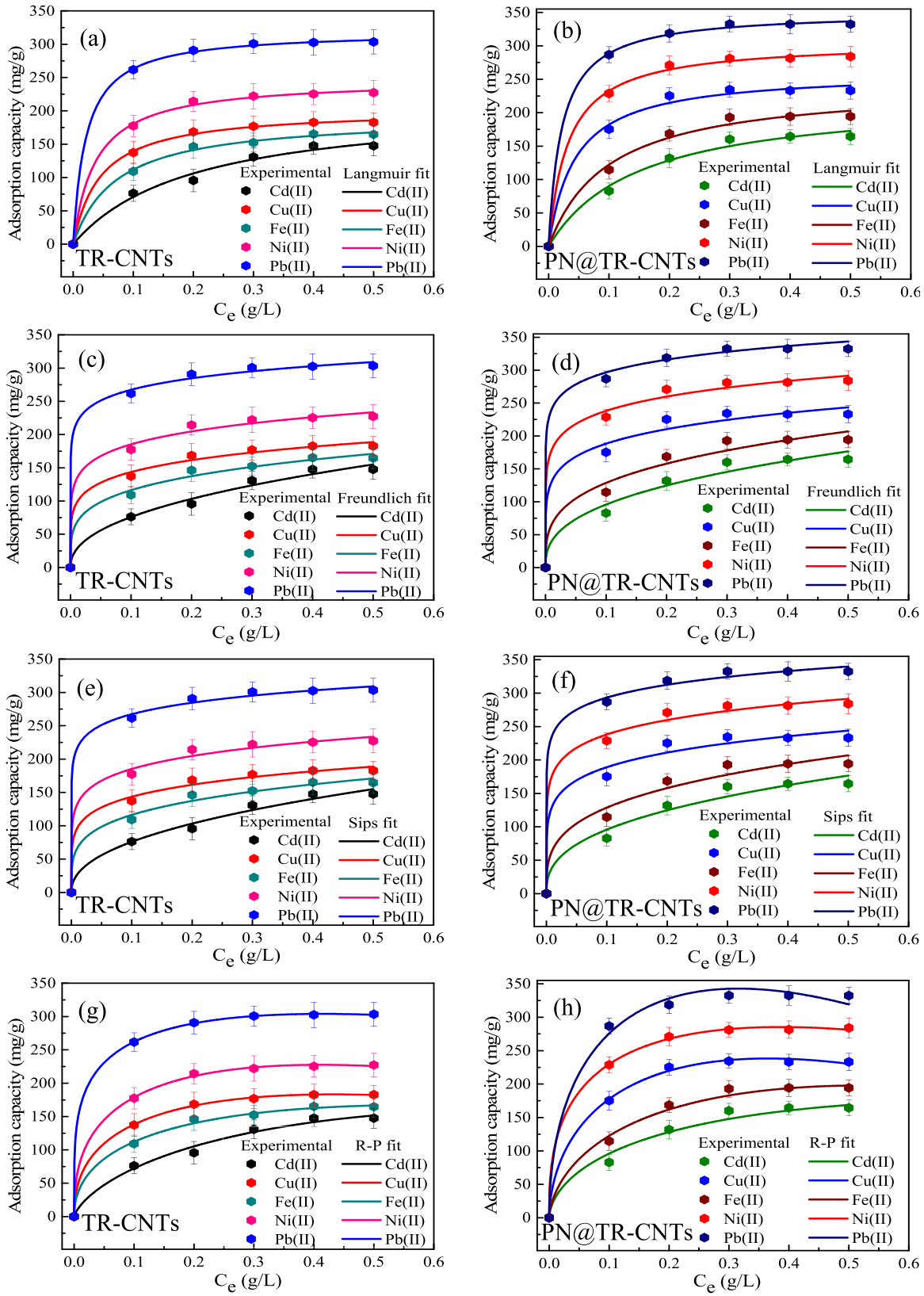

Fig. 5. Fitting of experimental isotherm data with Langmuir, Freundlich, Sips and Redlich-Peterson models using TR-CNTs (a, c, e and g) and PN@TR-CNTs (b, d, f and h) nanoadsorbents at pH (5 and 6), contact time (30 min) and temperature (303 K).

Table 2
Adsorption kinetic parameters for the adsorption of metal ions by TR-CNTs and PN@TR-CNTs.

Model/Mathematical Expression	Adsorbent	Parameters	Cd (II)	Cu (II)	Fe (II)	Ni (II)	Pb (II)
Pseudo-first order $q_t = q_e(1 - e^{-k_1 t})$	TR-CNTs	**q_e, (mg/g)**	136.155	170.508	153.990	215.335	298.342
		K_1 (1/min)	0.047	0.114	0.073	0.143	0.173
		R^2	0.959	0.893	0.990	0.754	0.652
		SSE	0.955	0.923	0.956	0.933	0.872
	PN@TR-CNTs	**q_e, (mg/g)**	147.594	182.323	168.039	225.388	299.626
		K_1 (1/min)	0.065	0.099	0.077	0.163	0.198
		R^2	0.964	0.992	0.980	0.990	0.995
		SSE	0.872	0.631	0.960	0.905	0.880
Pseudo-second order $q_t = \frac{k_2 q_e^2 t}{1 + k_2 q_e t}$	TR-CNTs	**q_e, (mg/g)**	165.103	185.830	174.558	229.963	311.611
		K_2 x 10^{-3}(1/min)	0.310	1.030	0.582	1.200	1.380
		R^2	0.986	0.995	0.999	0.997	0.999
		SSE	0.492	0.306	0.185	0.511	0.257
	PN@TR-CNTs	**q_e, (mg/g)**	170.178	199.966	189.876	237.160	310.521
		K_2 x 10^{-3}(g/mg.min)	0.499	0.811	0.559	1.551	1.782
		R^2	0.990	0.996	0.999	0.997	0.999
		SSE	0.266	0.441	0.306	0.120	0.481
Elovich $q_t = \frac{1}{\beta} \ln(1 + \alpha\beta t)$	TR-CNTs	**α (g/mg min)**	14.796	785.099	73.855	9024.411	17476.000
		β (mg/g)	0.026	0.045	0.034	0.047	0.052
		R^2	0.922	0.990	0.953	0.994	0.990
		SSE	2.044	5.180	4.417	8.331	7.833
	PN@TR-CNTs	**α (g/mg min)**	43.585	459.518	94.633	144205.331	413040.010
		β (mg/g)	0.032	0.039	0.032	0.058	0.063
		R^2	0.950	0.983	0.961	0.990	0.992
		SSE	1.307	8.682	3.650	5.322	4.306
Intraparticle diffusion $q_t = k_p t^{0.5} + C$	TR-CNTs	k_p	13.091	14.522	13.774	17.592	22.898
		C (mg/g)	16.743	54.500	37.353	77.046	118.885
		R^2	0.814	0.831	0.820	0.835	0.846
		SSE	18.499	27.938	24.611	45.440	36.521
	PN@TR-CNTs	k_p	13.541	15.485	15.018	17.707	22.708
		C (mg/g)	31.296	56.090	42.029	86.658	123.003
		R^2	0.830	0.844	0.836	0.855	0.878
		SSE	22.052	16.350	19.560	27.270	25.610

whereby qt (mg/g) is the amount of Cd(II), Cu(II), Fe(II), Ni(II) and Pb(II) ions adsorbed at a defined time; qe (mg/g) is the amount of Cd(II), Cu(II), Fe(II), Ni(II) and Pb (II) ions adsorbed at equilibrium; t (min) is the adsorption time; k1 (1/min) is the rate constant of the pseudo-first order model; k2 (g/mg min) is the rate constant of the pseudo-second order model; α (mg/g min) is the initial rate constant of Elovich model; β (mg/g) is the constant due to desorption; kp (mg/g·min0.5) is the rate constant of the intraparticle diffusion model and C (mg/g) is a constant correlated to the thickness of the boundary layer.

where k_d is the thermodynamic equilibrium constant, T (K) and R (J/mol/K) stand for the temperature in absolute scale and the universal gas constant, respectively. The plot of $\ln(q_e/C_e)$ on the y-axis and 1/T on the x-axis was used to investigate the mechanism behind the metal ions adsorption process onto the nanoadsorbents and determine the thermodynamic behaviour as shown in Fig. 7(a,b). The obtained slope from the plot was equal to $\Delta S/R$, whereas the intercept was equal to $-\Delta H/R$ [57]. Table 3 provides an overview of the thermodynamic parameter data. In general, the obtained negative ΔG° values show that the metal ion adsorption process on TR-CNTs and PN@TR-CNTs is spontaneous. Overall, an increase in temperature significantly decreased the values for the Gibbs free energy, corroborating a good adsorption capacity at 323 K using both nanoadsorbents.

Noticeably, the values of ΔH° were obtained in the range of 27.63–63.45 KJ/mol and 45.95–116.25 KJ/mol for the metal ions using both TR-CNTs and PN@TR-CNTs. Earlier, a previous study reported that values of ΔH° in the range of 1–40 KJ/mol indicate physisorption controlled adsorption process, while the values above 40 KJ/mol signify chemisorption controlled adsorption process [71]. In this regard, it is evident that metal ions adsorption by TR-CNTs was dominated by the physisorption process, while the adsorption of the metal ions by PN@TR-CNTs was the chemisorption-controlled process. Comparatively, the higher ΔH° values for Cd(II), Cu(II), Fe(II), Cd(II), and Pb(II) ions adsorption by TR-CNTs than PN@TR-CNTs revealed enhanced chemical interactions between the metal ions and the later nanoadsorbent, thereby corroborating to the higher adsorption capacity for the metal ions. Above all, the obtained values of ΔS° for TR-CNTs and PN@TR-CNTs were in the range of 76.20–160.81 J/mol.K and 184.17–448.52 J/mol.K, respectively. The trend of the positive values of ΔS° also affirmed a higher interaction between the metal ions and the porous surface of PN@TR-CNTs nanoadsorbent, than TR-CNTs nanoadsorbent [46]. Furthermore, the increasing randomness at the solid-liquid interface and the endothermic nature of the adsorption process are further suggested by the positive values of ΔS° and ΔH° [72].

3.7. Comparison study and limitations

The performance of TR-CNTs and PN@TR-CNTs towards the adsorption of the metal ions in this study was compared with different materials presented in Table 4.

Similarly, the adsorption parameters such as nanoadsorbent surface area, adsorption capacity, pH, contact time, adsorbent mass, initial metal concentrations, temperature, isotherm and kinetic model data were also highlighted. It is evident from the results that the TR-CNTs and PN@TR-CNTs exhibited a higher adsorption capacity towards the metal ions compared to other different adsorbents except for Cd(II) of 194.55 mg/g and Pb(II) of 434.70 mg/g using P(TA-MBA-GGQDs)/GeDN gel [19] and PANI-NSA@Ni°CNs [50]. In addition, this study achieved an improved adsorption capacity using a low nanoadsorbent mass (0.4 g/L), thus practically saving the materials. Remarkably, the equilibrium adsorption time of 60 min for the metal ions by the nanoadsorbents is an indication of time consumption effectiveness for the adsorption treatment. It can be recommended justifiably that TR-CNTs and PN@TR-CNTs are effective potential nanoadsorbent for the treatment of Cd(II), Cu(II), Fe(II), Ni(II) and Pb(II) from real wastewater.

Then again, some possible limitations of this study deserve to be mentioned. In the first instance, this study was basically on the laboratory experimental scale. A pilot study on the application of the TR-CNTs and PN@TR-CNTs nanoadsorbents is suggested to estimate the feasibility, applicability and overall cost of the real wastewater treatment. In

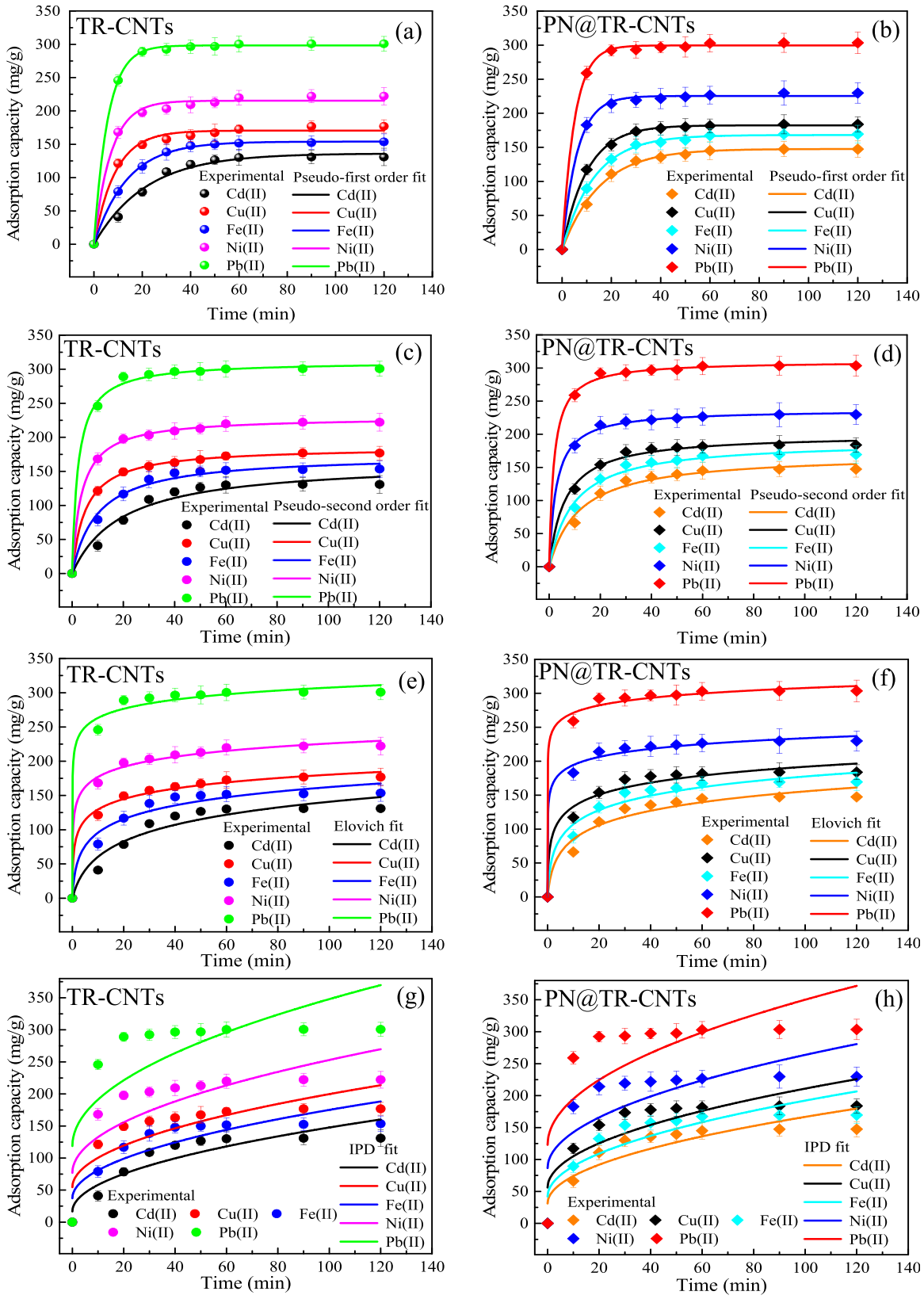

Fig. 6. Fitting of experimental kinetic data with pseudo-first order, pseudo-second order, Elovich and Intraparticle diffusion models using TR-CNTs (a, c, e and g) and PN@TR-CNTs (b, d, f and h) nanoadsorbents at pH (5 and 6), adsorbent dosage (0.4 g/L) and temperature (303 K).

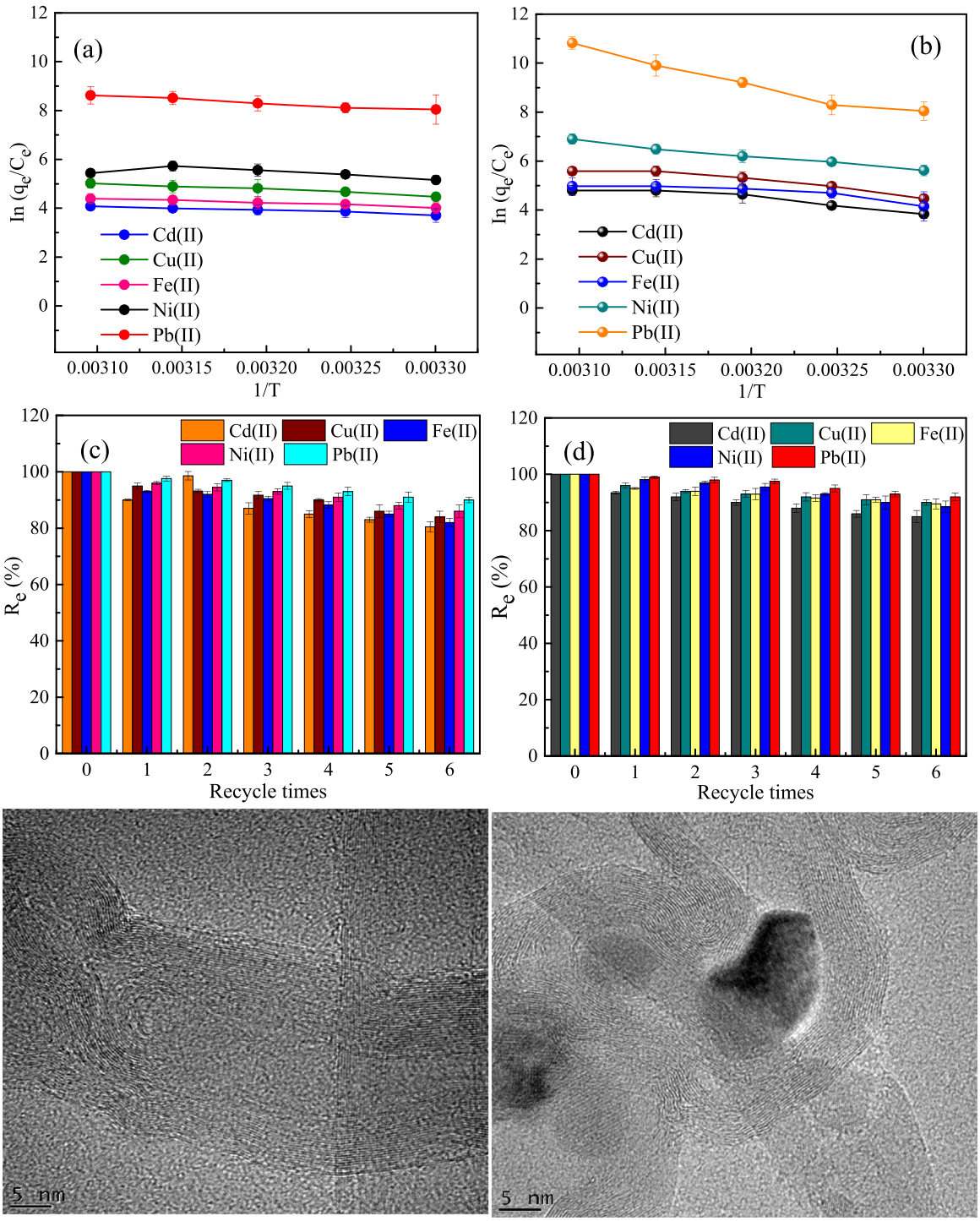

Fig. 7. Thermodynamic study for metal ions adsorption by (a) TR-CNTs; (b) PN@TR-CNTs at pH (5 and 6), nanoadsorbent dosage (0.4 g/L) and contact time (60 min); Reusability capacity of (c) TR-CNTs; (d) PN@TR-CNTs (adsorption conditions; pH (5 for Ni(II) and Pb(II), 6 for Cd(II), Cu(II) and Fe(II), nanoadsorbent dosage (0.4 g/L), initial metal concentration (0.1 g/L), contact time (60 min) and temperature (323 K)); HRTEM micrographs after the 6th recycle period of the metal ions adsorption using (e) TR-CNTs and (f) PN@TR-CNTs.

addition, further discussion on the treatment of the nanoadsorbents after reuse is required. Moreover, the prevention of secondary pollution by incinerating the expired nanoadsorbents may be adopted as a disposal technique, while considering other methods such as the conversion to catalysts, support materials and electronic materials to enhance a circular economy. In the future, it is expected that further studies will improve the performance of purified and functionalized CNTs in different applications such as drug delivery, fuel cells, catalysts and robust sensors.

3.8. *Reusability of nanoadsorbents*

The reusability of nanoadsorbents is a prominent factor that determines their sustainability and cost efficiency for commercial applications. The recyclability of TR-CNTs and PN@TR-CNTs towards the metal ions adsorption efficiency was investigated as a function of recycle

Table 3
Thermodynamic parameters of heavy metals adsorption by (a) TR-CNTs and (b) PN@TR-CNTs.

(a)										
T (K)	Cd (II)		Cu (II)		Fe (II)		Ni (II)		Pb (II)	
	k_d	ΔG° (J/mol)	k_d	ΔG° (J/mol)	k_d	ΔG° (J/mol)	k_d	ΔG° (J/mol)	k_d	ΔG° (J/mol)
303	40.56	-9.33	86.71	-11.24	55.27	-10.11	173.82	-57.99	3115.00	-90.43
308	47.67	-9.90	106.69	-11.96	64.35	-10.66	217.27	-64.35	3323.33	-96.97
313	51.09	-10.24	123.33	-12.53	68.37	-10.99	259.54	-69.65	3990.00	-103.89
318	54.27	-10.56	132.86	-12.93	76.51	-11.47	306.46	-74.01	4990.00	-110.07
323	58.97	-10.95	151.29	-13.48	80.83	-11.80	230.38	-73.32	5545.56	-116.20
ΔH° (KJ/mol)	27.63		31.57		38.09		46.29		63.45	
ΔS° (J/mol.K)	76.20		95.55		80.24		115.02		160.81	
(b)										
T(K)	Cd(II)		Cu(II)		Fe(II)		Ni(II)		Pb(II)	
	k_d	ΔG° (J/mol)	k_d	ΔG° (J/mol)	k_d	ΔG° (J/mol)	k_d	ΔG° (J/mol)	k_d	ΔG° (J/mol)
303	46.24	-9.33	86.71	-11.24	63.15	-10.04	275.71	-63.17	3115.00	-90.43
308	65.53	-10.71	144.80	-12.74	109.62	-11.42	390.00	-76.01	3990.00	-105.64
313	103.38	-12.07	202.77	-13.82	131.04	-12.69	490.00	-85.63	9990.00	-127.30
318	121.58	-12.69	268.55	-14.79	144.80	-12.94	656.67	-95.93	19990.00	-146.44
323	121.58	-12.89	268.55	-15.02	144.80	-13.89	990.00	-103.60	49990.00	-162.51
ΔH° (KJ/mol)	46.11		47.12		45.95		50.03		116.25	
ΔS° (J/mol.K)	184.17		193.73		185.76		211.73		448.52	

Table 4
Comparison of selected metal ions adsorption performance of TR-CNTs and PN@TR-CNTs with several adsorbents reported by the previous works.

Adsorbent	Surface area (m^2/g)	Metal ion	q_m (mg/g)	pH	Contact time (min)	Adsorbent dosage (g/L)	Initial concentration (mg/L)	Temperature (K)	Isotherm model	Kinetic model	Reference
P(TA-MBA-GGQDs)/GeDN gel	0.20	Cd(II) Pb(II)	194.55 259.07	5	300	–	1000	298	Langmuir	PSO[a]	[19]
SPES/MWCNTs	54.02	Pb(II)	54.05	6	35	0.50	100	298	Langmuir	PFO[b] PSO	[76]
Fe_2O_3-MWCNTs		Pb(II)	67.25	5	360	0.05	200	298	Langmuir	PFO	[77]
Fe_2O_3-Carbon Foam	458.59	Cu(II) Ni(II)	3.80 6.40	5 7	120	0.01	50	298	–	–	[2]
PANI-NSA@Ni°CNs	49.84	Pb(II)	434.70	5	90	0.50	150	288	Langmuir	PSO	[50]
TL	60.30	Cd(II) Cu(II) Ni(II)	3.70 2.80 2.00	6	–	0.01	5	318	Freundlich	PD[c]	[78]
MGBW	–	Fe(II) Cu(II) Ni(II)	7.60 6.70 6.20	8 8 6	60	2.00	200	303 313	Langmuir Freundlich	IPD[d]	[40]
PPTU	–	Cu(II) Ni(II) Cd(II) Pb(II) Fe(II)	9.40 12.60 90.90 57.10 30.40	6 6 9 5 6	30	0.12	160	298	Freundlich	PSO	[8]
Fe_2O_3		Cd(II) Pb(II)	25.84 9.01	5.5	120	5.00	20	298	Langmuir	PSO	[79]
BC-MnO_3	181.90	Cd(II)	151.43	4.5	1440	0.03	150	298	Langmuir	PSO	[80]
TR-CNTs/PN@TR-CNTs	970.81/781.88	Cd(II) Cu(II) Fe(II) Ni(II) Pb(II)	147.60/164.44 182.82/233.12 165.30/194.54 225.29/283.47 302.53/323.43	6 6 6 5 5	60	0.40	100	323	Redlich-Peterson	PSO	Present study

NB: a refers to Pseudo-second order; b refers to Pseudo-first order: c refers to pore diffusion and d intraparticle diffusion.

times and the results are presented in Fig. 7(c,d). It was observed that during the first 4 cycles, the adsorption efficiency of Cd(II), Cu(II), Fe (II), Ni(II) and Pb(II) gradually declined from 90.2% to 85.1%, 95.2–90.3%, 93.2–88.2%, 96.0–91.4% and 97.6–93.3% using TR-CNTs and stabilized eventually at 80.5%, 84.2%, 82.4%, 86.1% and 90.2% after 6 adsorption cycles. Similarly, the recyclability study of PN@TR-CNTs towards Cd(II), Cu(II), Fe(II), Ni(II) and Pb(II) revealed a declining adsorption efficiency from 93.5% to 88.0%, 96.0–92.0%, 95.0–91.6%, 98.1–93.0% and from 99.0% to 95.0% until stabilization at 85.0%, 90.1%, 89.5%, 88.5% and 92.0% after 6 recycle times. Remarkably, the adsorption efficiency of the metal ions using TR-CNTs and PN@TR-CNTs was over 80.0% and 85.2% even after the 6 recycle

times. The HRTEM micrographs in Fig. 7(e,f) showed that the microstructures of TR-CNTs and PN@TR-CNTs maintained an overall microstructural network, indicating a preserved surface of the nanoadsorbents after 6 cycles of reuse. These results indicate that TR-CNTs and PN@TR-CNTs micrographs could be used for the multiple treatments of Cd(II), Cu(II), Fe(II), Ni(II) and Pb(II) ions containing electroplating wastewater, thereby reducing cost management.

3.9. Adsorption mechanism

The adsorption mechanism largely depends on the nanoadsorbent properties such as surface area, porous surface, functional groups and optimum adsorption conditions. The adsorption mechanism that primarily occurs in nanoadsorbents includes pore filling, electrostatic interaction, hydrogen bonding and surface complexation [73–75]. The evaluation of the dominant possible adsorption mechanism was conducted on the nanoadsorbents properties through correlation analysis and characterization as shown in Fig. 8.

The intraparticle diffusion kinetics were satisfactorily fitted ($R^2 = > 0.810$) (Table 2), indicating that pore filling contributed positively to the adsorption mechanism of metal ions adsorption onto TR-CNTs and PN@TR-CNTs. After Cd(II), Cu(II), Fe(II), Ni(II) and Pb(II) adsorption, the BET surface properties of the nanoadsorbents were measured as shown in Table S1. It is evident that the surface area, pore size and pore volume of the nanoadsorbents decreased, indicating that Cd(II), Cu(II), Fe(II), Ni(II) and Pb(II) ions occupied the available active binding sites and the blockage of the adsorption channels of the TR-CNTs and PN@TR-CNTs. This investigation showed that the metal ions adsorption occurred majorly on the external and internal porous surface of the nanoadsorbents, an implication that pores filling was the dominant mechanism for the metal ions adsorption on the nanoadsorbents.

Based on the influence of pH on the metal ions adsorption, the electrostatic interaction contributions to the adsorption process were explored (Fig. 3f). As can be seen, the TR-CNTs and PN@TR-CNTs had a zero point of zeta potential at pH 4.5 and 5, showing that the nanoadsorbents had a negative zeta potential under weak acidic, neutral and basic conditions. As such, the negative zeta potential of the nanoadsorbents enhances the adsorption of the metal ions carrying positive zeta potentials in solutions. Hence, the adsorption of Cd(II), Cu(II), Fe (II), Ni(II) and Pb(II) increased with pH values increment from 4.5/5–6. The improved performance of the nanoadsorbents at this pH range was due to less repulsive and more attractive electrostatic interactions between TR-CNTs/PN@TR-CNTs and metal ions. As shown in Fig. 8, the nanoadsorbents surface contains functional groups such as -OH, -CHO, -NH and -COOH. These functional groups were attributed to the occurrence of hydrogen bonding, electrostatic interaction and surface complexation on the surface of the nanoadsorbents. Similarly, the protonated surface of the nanoadsorbents provoked the adsorption of Cd (II), Cu(II), Fe(II), Ni(II) and Pb(II) on the TR-CNTs and PN@TR-CNTs through the occurrence of electrostatic attraction and hydrogen bonding. The results of the above analysis confirmed that the adsorption mechanisms were typically by pore filling and electrostatic attraction, followed by hydrogen bonding and surface complexation.

4. Conclusion and future directions

In this study, CNTs were successfully synthesized on Fe-Ni/kaolin supported catalyst using the CVD technique before purification and

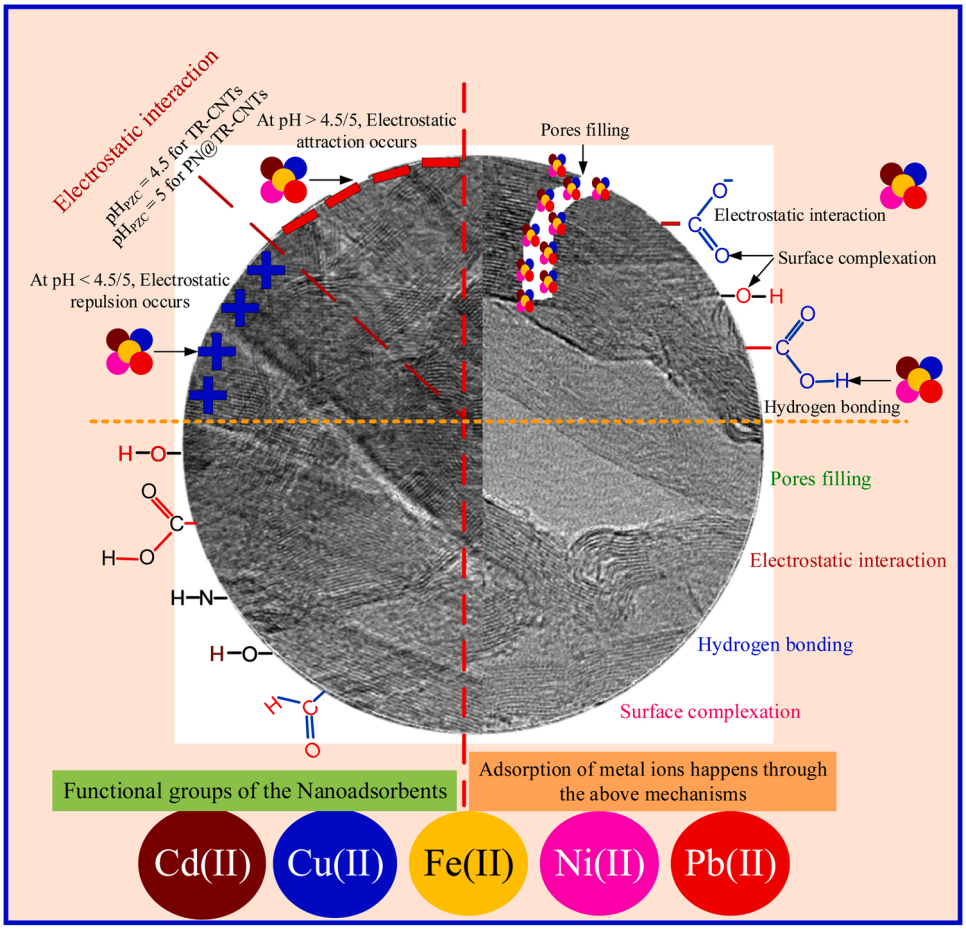

Fig. 8. Proposed adsorption mechanism of metal ions by the nanoadsorbents.

functionalization to obtain TR-CNTs and PN@TR-CNTs. The characterization of the nanoadsorbents was conducted using XRD, FTIR, HRSEM, HRTEM, EDX and surface properties measurement. The systematic adsorption performance and mechanism of Cd(II), Cu(II), Fe(II), Ni(II) and Pb(II) in electroplating wastewater were investigated. The results of the characterization indicate successful fabrication of CNTs, and purification and functionalization of the CNTs surface properties. The adsorption of the metal ions was optimized at pH of 5 for Ni(II)/Pb(II) and 6 for Cd(II)/Cu(II)/Fe(II), contact time of 60 min, nanoadsorbent dosage of 0.4 g/L and temperature of 50 °C. Moreover, the isotherm and kinetic adsorption of the metal ions adhered to Redlich-Peterson and pseudo second-order models, respectively. The maximum adsorption capacities for Cd(II), Cu(II), Fe(II), Ni(II), and Pb(II) were obtained as 147.60, 182.82, 165.30, 225.29 and 302.53 mg/g using TR-CNTs, while 164.44, 233.12, 194.54, 283.47 and 332.43 mg/g were determined for Cd(II), Cu(II), Fe(II), Ni(II), and Pb(II) adsorption onto PN@TR-CNTs. The TR-CNTs and PN@TR-CNTs could be reused repeatedly for 6 adsorption-desorption cycles, providing higher adsorption capacity than other previous materials. The adsorption mechanism of the metal ions by the nanoadsorbents was predominantly by pore filling and electrostatic attraction, followed by hydrogen bonding and surface complexation. Based on the outstanding adsorption performance of the nanoadsorbents and reusability effectiveness for practical application, the study explores the great potential of purified and functionalized CNTs to efficiently remove metal ions from electroplating wastewater. This study contributes immensely to the development of new generation nanoadsorbents, as well as providing directions for promising future research.

CRediT authorship contribution statement

Ambali Saka Abdulkareem: Conceptualization, Investigation, Methodology, Data curation, Writing – original draft, Writing – review & editing, Validation. **Wasiu Abidemi Hamzat:** Investigation, Methodology, Data curation, Writing – original draft, Writing – review & editing. **Jimoh Oladejo Tijani:** Data curation, Writing – review & editing. **Titus Chinedu Egbosiuba:** Investigation, Methodology, Data curation, Writing – original draft, Writing – review & editing, Validation. **Saheed Mustapha:** Writing – review & editing, Resources, Supervision. **Oladiran Kamardeen Abubakre:** Characterization, Resources, Supervision. **Blessing Onyinye Okafor:** Data curation, Methodology, Software. **Akinpelu Kamoru Babayemi:** Data curation, Methodology, Software.

Declaration of Competing Interest

The authors declare that they have no known competing financial interests or personal relationships that could have appeared to influence the work reported in this paper.

Data Availability

Data will be made available on request.

Acknowledgements

This work was financially supported by Tertiary Education Trust Fund, Nigeria (TETFUND/FUTMINNA/NRF/2014/01 and TETFUND/FUTMINNA/2019/B7/16) and African Centre of Excellence on Mycotoxins, Federal University of Technology, Minna, Nigeria.

Appendix A. Supporting information

Supplementary data associated with this article can be found in the online version at doi:10.1016/j.jece.2022.109180.

References

[1] P. Sharma, D. Dutta, A. Udayan, S. Kumar, Industrial wastewater purification through metal pollution reduction employing microbes and magnetic nanocomposites, J. Environ. Chem. Eng. 9 (2021), 106673, https://doi.org/10.1016/j.jece.2021.106673.

[2] C.G. Lee, S. Lee, J.A. Park, C. Park, S.J. Lee, S.B. Kim, B. An, S.T. Yun, S.H. Lee, J. W. Choi, Removal of copper, nickel and chromium mixtures from metal plating wastewater by adsorption with modified carbon foam, Chemosphere 166 (2017) 203–211, https://doi.org/10.1016/j.chemosphere.2016.09.093.

[3] B. Kabak, E. Kendüzler, Synthesis, characterization and adsorption/sensing applications of novel cadmium(II) based coordination polymer, J. Environ. Chem. Eng. 10 (2022), 107989, https://doi.org/10.1016/j.jece.2022.107989.

[4] M. Shahabi Nejad, H. Sheibani, Super-efficient removal of arsenic and mercury ions from wastewater by nanoporous biochar-supported poly 2-aminothiophenol, J. Environ. Chem. Eng. 10 (2022), 107363, https://doi.org/10.1016/j.jece.2022.107363.

[5] H. Masoumi, A. Ghaemi, H. Gannadzadeh Gilani, Synthesis of polystyrene-based hyper-cross-linked polymers for Cd(II) ions removal from aqueous solutions: Experimental and RSM modeling, J. Hazard. Mater. 416 (2021), 125923, https://doi.org/10.1016/j.jhazmat.2021.125923.

[6] T.C. Egbosiuba, A.S. Abdulkareem, A.S. Kovo, E.A. Afolabi, J.O. Tijani, M. T. Bankole, S. Bo, W.D. Roos, Adsorption of Cr(VI), Ni(II), Fe(II) and Cd(II) ions by KIAgNPs decorated MWCNTs in a batch and fixed bed process, Sci. Rep. 11 (2021) 1–20, https://doi.org/10.1038/s41598-020-79857-z.

[7] A.A. Castañeda-Ramírez, E. Rojas-García, R. López-Medina, D.C. García-Martínez, J. Nicolás- Antúnez, A.M. Maubert-Franco, Magnetite nanoparticles into Fe-BTC MOF as adsorbent material for the remediation of metal (Cu(II), Pb(II, As(III) and Hg(II)) ions-contaminated water, Catal. Today 394– 396 (2022) 94–102, https://doi.org/10.1016/j.cattod.2021.11.007.

[8] Ş. Uçak, A. Aydın, A novel thiourea derivative for preconcentration of copper(II), nickel(II), cadmium(II), lead(II) and iron(II) from seawater samples for Flame Atomic Absorption Spectrophotometry, Mar. Pollut. Bull. 180 (2022), https://doi.org/10.1016/j.marpolbul.2022.113787.

[9] G. Mokokwe, M.W. Letshwenyo, Utilisation of cement brick waste as low cost adsorbent for the adsorptive removal of copper, nickel and iron from aqueous solution: batch and column studies, Phys. Chem. Earth. 126 (2022), 103156, https://doi.org/10.1016/j.pce.2022.103156.

[10] J. Qu, X. Tian, Z. Jiang, B. Cao, M.S. Akindolie, Q. Hu, C. Feng, Y. Feng, X. Meng, Y. Zhang, Multi-component adsorption of Pb(II), Cd(II) and Ni(II) onto microwave-functionalized cellulose: kinetics, isotherms, thermodynamics, mechanisms and application for electroplating wastewater purification, J. Hazard. Mater. 387 (2020), https://doi.org/10.1016/j.jhazmat.2019.121718.

[11] WHO, Guidelines for Drinking-water Quality, Fourth Ed. (2017) 631. https://doi.org/10.1016/S1462–0758(00)00006–6.

[12] J.O. Tijani, M.N. Abdullahi, M.T. Bankole, S. Mustapha, T.C. Egbosiuba, M. M. Ndamitso, A.S. Abdulkareem, E. Muzenda, Photocatalytic and toxicity evaluation of local dyeing wastewater by aluminium/boron doped WO3 nanoparticles, J. Water Process Eng. 44 (2021), 102376, https://doi.org/10.1016/j.jwpe.2021.102376.

[13] S. Sagadevan, I. Fatimah, T.C. Egbosiuba, S.F. Alshahateet, J.A. Lett, G. K. Weldegebrieal, M.-V. Le, M.R. Johan, Photocatalytic efficiency of titanium dioxide for dyes and heavy metals removal from wastewater, Bull. Chem. React. Eng. Catal. 17 (2022) 430–450, https://doi.org/10.9767/bcrec.17.2.13948.430-450.

[14] O. Onukwuli, P. Nnaji, M. Menkiti, V.C. Anadebe, E. Oke, C.N. Ude, C.J. Ude, N. A. Okafor, Dual-purpose optimization of dye-polluted wastewater decontamination using bio-coagulants from multiple processing techniques via neural intelligence algorithm and response surface methodology, J. Taiwan Inst. Chem. Eng. (2021), https://doi.org/10.1016/J.JTICE.2021.06.030.

[15] A.S. Meltzer, A.J. Sci, M.R. Strecker, E. Planet, S. Lett, organic solvents from high-value products such as pharmaceuticals (4). However, organic solvent nanofiltration membrane materials do not have the necessary molecular specificity to efficiently, Sci. (80-.) (2016) 02403.

[16] A.B. Rostam, M. Taghizadeh, Advanced oxidation processes integrated by membrane reactors and bioreactors for various wastewater treatments: a critical review, J. Environ. Chem. Eng. 8 (2020), 104566, https://doi.org/10.1016/j.jece.2020.104566.

[17] J.O. Tijani, E.I. Odeh, S. Mustapha, T.C. Egbosiuba, A.I. Daniel, A.S. Abdulkareem, F.N. Muya, Photocatalytic, electrochemical, antibacterial and antioxidant behaviour of carbon-sulphur Co-doped zirconium (IV) oxide nanocomposite, Clean Chem. Eng. (2022), 100034, https://doi.org/10.1016/j.clce.2022.100034.

[18] C.A. Uko, J.O. Tijani, S.A. Abdulkareem, S. Mustapha, T.C. Egbosiuba, E. Muzenda, Adsorptive properties of MgO/WO3 nanoadsorbent for selected heavy metals removal from indigenous dyeing wastewater, Process Saf. Environ. Prot. 162 (2022) 775–794, https://doi.org/10.1016/j.psep.2022.04.057.

[19] S. Lai, Y. Jin, L. Shi, Y. Li, R. Zhou, Tailoring multifunctional gel for sensitive naked-eye and fluorescence dual-mode detection and effective adsorption of cadmium(II) and lead(II) ions in water, Chem. Eng. J. 429 (2022), 132367, https://doi.org/10.1016/j.cej.2021.132367.

[20] R. Kumar, S. Bhattacharya, P. Sharma, Novel insights into adsorption of heavy metal ions using magnetic graphene composites, J. Environ. Chem. Eng. 9 (2021), 106212, https://doi.org/10.1016/j.jece.2021.106212.

[21] T.C. Egbosiuba, Application of agricultural waste in anionic dyes removal from wastewater, Text. Waste Water Treat. (2022).

[22] T.C. Egbosiuba, Biochar and bio-oil fuel properties from nickel nanoparticles assisted pyrolysis of cassava peel, Heliyon 8 (2022), e10114, https://doi.org/10.1016/j.heliyon.2022.e10114.
[23] A.E. Burakov, E.V. Galunin, I.V. Burakova, A.E. Kucherova, S. Agarwal, A. G. Tkachev, V.K. Gupta, Adsorption of heavy metals on conventional and nanostructured materials for wastewater treatment purposes: a review, Ecotoxicol. Environ. Saf. 148 (2018) 702–712, https://doi.org/10.1016/j.ecoenv.2017.11.034.
[24] D.Y. Koh, B.R. Pimentel, V.P. Babu, N. Stephenson, S.W. Chai, A. Rosinski, R. P. Lively, Sub-ambient air separation via Li+ exchanged zeolite, Microporous Mesoporous Mater. 256 (2018) 140–146, https://doi.org/10.1016/j.micromeso.2017.06.028.
[25] K. Kim, Y.E. Hwang, Y.H. Lee, S.J. Park, D. Kim, D.Y. Koh, All-Nanoporous fiber sorbent with a Non-Sacrificial polymer of intrinsic microporosity (PIM) matrix, Sep. Purif. Technol. 289 (2022), https://doi.org/10.1016/j.seppur.2022.120639.
[26] J. Ifthikar, I.I. Shahib, L. Sellaoui, A. Jawad, M. Zhao, Z. Chen, Z. Chen, pH tunable anionic and cationic heavy metal reduction coupled adsorption by thiol cross-linked composite: Physicochemical interpretations and fixed-bed column mathematical model study, Chem. Eng. J. 401 (2020), https://doi.org/10.1016/j.cej.2020.126041.
[27] M.A. Ganzoury, C. Chidiac, J. Kurtz, C.F. de Lannoy, CNT-sorbents for heavy metals: electrochemical regeneration and closed-loop recycling, J. Hazard. Mater. 393 (2020), 122432, https://doi.org/10.1016/j.jhazmat.2020.122432.
[28] S.Z.N. Ahmad, W.N. Wan Salleh, A.F. Ismail, N. Yusof, M.Z. Mohd Yusop, F. Aziz, Adsorptive removal of heavy metal ions using graphene-based nanomaterials: toxicity, roles of functional groups and mechanisms, Chemosphere 248 (2020), 126008, https://doi.org/10.1016/J.CHEMOSPHERE.2020.126008.
[29] D. Jia, Z. Jing, Y. Duan, J. Li, Ultrafast removal of Cr(VI) ions using polyamine modified carbon nanotubes, J. Taiwan Inst. Chem. Eng. 133 (2022), 104265, https://doi.org/10.1016/j.jtice.2022.104265.
[30] T.C. Egbosiuba, A.S. Abdulkareem, A.S. Kovo, E.A. Afolabi, J.O. Tijani, W.D. Roos, Enhanced adsorption of As(V) and Mn(VII) from industrial wastewater using multi-walled carbon nanotubes and carboxylated multi-walled carbon nanotubes, Chemosphere 254 (2020), 126780, https://doi.org/10.1016/j.chemosphere.2020.126780.
[31] T.C. Egbosiuba, Incorporation of zero-valent silver and polyvinyl acetate on the surface matrix of carbon nanotubes for the adsorption of mercury and chromium from industrial wastewater, Niger. J. Technol. 41 (2022) 158–168.
[32] M.T. Bankole, A.S. Abdulkareem, I.A. Mohammed, S.S. Ochigbo, J.O. Tijani, O. K. Abubakre, W.D. Roos, Selected heavy metals removal from electroplating wastewater by purified and polyhydroxylbutyrate functionalized carbon nanotubes adsorbents, Sci. Rep. 9 (2019) 1–19, https://doi.org/10.1038/s41598-018-37899-4.
[33] A. ZabihiSahebi, S. Koushkbaghi, M. Pishnamazi, A. Askari, R. Khosravi, M. Irani, Synthesis of cellulose acetate/chitosan/SWCNT/Fe3O4/TiO2 composite nanofibers for the removal of Cr(VI), As(V), Methylene blue and Congo red from aqueous solutions, Int. J. Biol. Macromol. 140 (2019) 1296–1304, https://doi.org/10.1016/j.ijbiomac.2019.08.214.
[34] V. Krstić, T. Urošević, B. Pešovski, A review on adsorbents for treatment of water and wastewaters containing copper ions, Chem. Eng. Sci. 192 (2018) 273–287, https://doi.org/10.1016/j.ces.2018.07.022.
[35] H. Sadegh, K. Zare, B. Maazinejad, R. Shahryari-Ghoshekandi, I. Tyagi, S. Agarwal, V.K. Gupta, Synthesis of MWCNT-COOH-Cysteamine composite and its application for dye removal, J. Mol. Liq. 215 (2016) 221–228, https://doi.org/10.1016/j.molliq.2015.12.042.
[36] V.K. Gupta, T.A. Saleh, Sorption of pollutants by porous carbon, carbon nanotubes and fullerene- an overview, Environ. Sci. Pollut. Res. 20 (2013) 2828–2843, https://doi.org/10.1007/s11356-013-1524-1.
[37] T.C. Egbosiuba, A.S. Abdulkareem, Highly efficient as-synthesized and oxidized multi-walled carbon nanotubes for copper(II) and zinc(II) ion adsorption in a batch and fixed-bed process, J. Mater. Res. Technol. 15 (2021) 2848–2872, https://doi.org/10.1016/j.jmrt.2021.09.094.
[38] C. Bai, L. Wang, Z. Zhu, Adsorption of Cr(III) and Pb(II) by graphene oxide/alginate hydrogel membrane: Characterization, adsorption kinetics, isotherm and thermodynamics studies, Int. J. Biol. Macromol. 147 (2020) 898–910, https://doi.org/10.1016/j.ijbiomac.2019.09.249.
[39] M. Zhao, Z. Huang, S. Wang, L. Zhang, Ultrahigh efficient and selective adsorption of Au(III) from water by novel Chitosan-coated MoS2 biosorbents: performance and mechanisms, Chem. Eng. J. 401 (2020), 126006, https://doi.org/10.1016/j.cej.2020.126006.
[40] G. Mokokwe, M.W. Letshwenyo, Investigation of clay brick waste for the removal of copper, nickel and iron from aqueous solution: batch and column studies, SSRN Electron. J. 8 (2022), e09963, https://doi.org/10.2139/ssrn.4044596.
[41] F. Marrakchi, B.H. Hameed, M. Bouaziz, Mesoporous and high-surface-Area activated carbon from defatted olive cake by-products of olive mills for the adsorption kinetics and isotherm of methylene blue and acid blue 29, J. Environ. Chem. Eng. 8 (2020), https://doi.org/10.1016/j.jece.2020.104199.
[42] T.C. Egbosiuba, A.S. Abdulkareem, J.O. Tijani, J.I. Ani, V. Krikstolaityte, M. Srinivasan, A. Veksha, G. Lisak, Taguchi optimization design of diameter-controlled synthesis of multi walled carbon nanotubes for the adsorption of Pb(II) and Ni(II) from chemical industry wastewater, Chemosphere 266 (2021), 128937, https://doi.org/10.1016/j.chemosphere.2020.128937.
[43] A.M. Abdelghany, M.S. Meikhail, N. Asker, Synthesis and structural-biological correlation of PVC\PVAc polymer blends, J. Mater. Res. Technol. 8 (2019) 3908–3916, https://doi.org/10.1016/j.jmrt.2019.06.053.
[44] Y. Hu, L. Zhang, P. Zhao, C. Wang, J. Fei, Y. Xie, Ultrasensitive luteolin electrochemical sensor based on zeolitic imidazolate frameworks-derived cobalt trioxide @ nitrogen doped carbon nanotube/amino-functionalized graphene quantum dots composites modified glass carbon electrode, Sens. Actuators B Chem. 351 (2022), 130938, https://doi.org/10.1016/j.snb.2021.130938.
[45] V.D. Doan, M.T. Phung, T.L.H. Nguyen, T.C. Mai, T.D. Nguyen, Noble metallic nanoparticles from waste Nypa fruticans fruit husk: Biosynthesis, characterization, antibacterial activity and recyclable catalysis, Arab. J. Chem. 13 (2020) 7490–7503, https://doi.org/10.1016/j.arabjc.2020.08.024.
[46] R. Mogale, K.G. Akpomie, J. Conradie, E.H.G. Langner, Dye adsorption of aluminium- and zirconium-based metal organic frameworks with azobenzene dicarboxylate linkers, J. Environ. Manag. 304 (2022), 114166, https://doi.org/10.1016/j.jenvman.2021.114166.
[47] S. Niu, J. Cheng, Y. Zhao, M. Kang, Y. Liu, Preparation and characterization of multifunctional phase change material microcapsules with modified carbon nanotubes for improving the thermal comfort level of buildings, Constr. Build. Mater. 347 (2022), 128628, https://doi.org/10.1016/j.conbuildmat.2022.128628.
[48] B. Duan, Y. Zhou, D. Wang, Y. Zhao, Effect of CNTs content on the microstructures and properties of CNTs/Cu composite by microwave sintering, J. Alloy. Compd. 771 (2019) 498–504, https://doi.org/10.1016/j.jallcom.2018.08.315.
[49] K.V.M.K. Kireeti, N. Jha, Surface tailored single walled carbon nanotubes as catalyst support for direct methanol fuel cell, J. Power Sources 364 (2017) 392–399, https://doi.org/10.1016/j.jpowsour.2017.08.019.
[50] M. Bhaumik, A. Maity, H.G. Brink, Zero valent nickel nanoparticles decorated polyaniline nanotubes for the efficient removal of Pb(II) from aqueous solution: Synthesis, characterization and mechanism investigation, Chem. Eng. J. 417 (2021), https://doi.org/10.1016/j.cej.2020.127910.
[51] M.E. Malool, M. KeshavarzMoraveji, J. Shayegan, Hydrothermal carbonization of digested sewage sludge coupled with Alkali activation: Integrated approach for sludge handling, optimized production, characterization and Pb(II) adsorption, J. Taiwan Inst. Chem. Eng. 133 (2022), https://doi.org/10.1016/j.jtice.2022.104203.
[52] T.C. Egbosiuba, M. Chika, J. Oladejo, S. Mustapha, A. Saka, A. Sanni, Activated multi-walled carbon nanotubes decorated with zero valent nickel nanoparticles for arsenic, cadmium and lead adsorption from wastewater in a batch and continuous flow modes, J. Hazard. Mater. 423 (2022), 126993, https://doi.org/10.1016/j.jhazmat.2021.126993.
[53] L. Sellaoui, D.I. Mendoza-Castillo, H.E. Reynel-Ávila, B.A. Ávila-Camacho, L. L. Díaz-Muñoz, H. Ghalla, A. Bonilla-Petriciolet, A. Ben Lamine, Understanding the adsorption of Pb2+, Hg2+ and Zn2+ from aqueous solution on a lignocellulosic biomass char using advanced statistical physics models and density functional theory simulations, Chem. Eng. J. 365 (2019) 305–316, https://doi.org/10.1016/j.cej.2019.02.052.
[54] Q. Chen, J. Zheng, L. Wen, C. Yang, L. Zhang, A multi-functional-group modified cellulose for enhanced heavy metal cadmium adsorption: Performance and quantum chemical mechanism, Chemosphere 224 (2019) 509–518, https://doi.org/10.1016/j.chemosphere.2019.02.138.
[55] X. Liu, J. Guan, G. Lai, Q. Xu, X. Bai, Z. Wang, S. Cui, Stimuli-responsive adsorption behavior toward heavy metal ions based on comb polymer functionalized magnetic nanoparticles, J. Clean. Prod. 253 (2020), 119915, https://doi.org/10.1016/j.jclepro.2019.119915.
[56] X. Huang, D.Y. Zemlyanov, S. Diaz-Amaya, M. Salehi, L. Stanciu, A.J. Whelton, Competitive heavy metal adsorption onto new and aged polyethylene under various drinking water conditions, J. Hazard. Mater. 385 (2020), 121585, https://doi.org/10.1016/j.jhazmat.2019.121585.
[57] S. Singh, A.G. Anil, S. Khasnabis, V. Kumar, B. Nath, V. Adiga, T.S.S. Kumar Naik, S. Subramanian, V. Kumar, J. Singh, P.C. Ramamurthy, Sustainable removal of Cr (VI) using graphene oxide-zinc oxide nanohybrid: Adsorption kinetics, isotherms and thermodynamics, Environ. Res. 203 (2022), 111891, https://doi.org/10.1016/j.envres.2021.111891.
[58] C. Patra, R. Gupta, D. Bedadeep, S. Narayanasamy, Surface treated acid-activated carbon for adsorption of anionic azo dyes from single and binary adsorptive systems: A detail insight, Environ. Pollut. 266 (2020), 115102, https://doi.org/10.1016/j.envpol.2020.115102.
[59] Y. Zhang, Y. Wang, H. Zhang, Y. Li, Z. Zhang, W. Zhang, Recycling spent lithium-ion battery as adsorbents to remove aqueous heavy metals: adsorption kinetics, isotherms, and regeneration assessment, Resour. Conserv. Recycl. 156 (2020), 104688, https://doi.org/10.1016/j.resconrec.2020.104688.
[60] P. Arabkhani, A. Asfaram, Development of a novel three-dimensional magnetic polymer aerogel as an efficient adsorbent for malachite green removal, J. Hazard. Mater. 384 (2020), 121394, https://doi.org/10.1016/j.jhazmat.2019.121394.
[61] U. Tyagi, Enhanced adsorption of metal ions onto Vetiveria zizanioides biochar via batch and fixed bed studies, Bioresour. Technol. 345 (2022), 126475, https://doi.org/10.1016/j.biortech.2021.126475.
[62] S. Tasharrofi, Z. Rouzitalab, D.M. Maklavany, A. Esmaeili, M. Rabieezadeh, M. Askarieh, A. Rashidi, H. Taghdisian, Adsorption of cadmium using modified zeolite-supported nanoscale zero-valent iron composites as a reactive material for PRBs, Sci. Total Environ. 736 (2020), https://doi.org/10.1016/j.scitotenv.2020.139570.
[63] G. Mokokwe, M.W. Letshwenyo, Utilisation of cement brick waste as low cost adsorbent for the adsorptive removal of copper, nickel and iron from aqueous solution: Batch and column studies, Phys. Chem. Earth 126 (2022), 103156, https://doi.org/10.1016/j.pce.2022.103156.
[64] M.A. Betiha, Y.M. Moustafa, A.S. Mansour, E. Rafik, M.F. El-Shahat, Nontoxic polyvinylpyrrolidone-propylmethacrylate-silica nanocomposite for efficient

adsorption of lead, copper, and nickel cations from contaminated wastewater, J. Mol. Liq. 314 (2020), https://doi.org/10.1016/j.molliq.2020.113656.
[65] M. Kavand, P. Eslami, L. Razeh, The adsorption of cadmium and lead ions from the synthesis wastewater with the activated carbon: optimization of the single and binary systems, J. Water Process Eng. 34 (2020), 101151, https://doi.org/10.1016/j.jwpe.2020.101151.
[66] S.S.A. Alkurdi, R.A. Al-Juboori, J. Bundschuh, L. Bowtell, A. Marchuk, Inorganic arsenic species removal from water using bone char: A detailed study on adsorption kinetic and isotherm models using error functions analysis, J. Hazard. Mater. 405 (2021), 124112, https://doi.org/10.1016/j.jhazmat.2020.124112.
[67] G. Zhang, L. Li, G. Zhou, Z. Lin, J. Wang, G. Wang, F. Ling, T. Liu, Recyclable aminophenylboronic acid modified bacterial cellulose microspheres for tetracycline removal: kinetic, equilibrium and adsorption performance studies for hoggery sewer, Environ. Pollut. 307 (2022), 119544, https://doi.org/10.1016/j.envpol.2022.119544.
[68] M. Xiong, M. Yang, Q. Chen, T. Cai, Mechanism studies for adsorption and extraction of soluble sodium from bauxite residue: characterization, kinetics, and thermodynamics, J. Environ. Chem. Eng. 10 (2022), 108183, https://doi.org/10.2139/ssrn.4085473.
[69] J. Qu, X. Tian, Z. Jiang, B. Cao, M. Sarah, Q. Hu, C. Feng, Y. Feng, X. Meng, Y. Zhang, Multi-component adsorption of Pb (II), Cd (II) and Ni (II) onto microwave- functionalized cellulose: kinetics, isotherms, thermodynamics, mechanisms and application for electroplating wastewater puri fi cation, J. Hazard. Mater. (2019).
[70] T.C. Egbosiuba, A.S. Abdulkareem, A.S. Kovo, E.A. Afolabi, J.O. Tijani, M. Auta, W. D. Roos, Ultrasonic enhanced adsorption of methylene blue onto the optimized surface area of activated carbon: adsorption isotherm, kinetics and thermodynamics, Chem. Eng. Res. Des. 153 (2020), https://doi.org/10.1016/j.cherd.2019.10.016.
[71] S. Cheng, L. Zhang, H. Xia, J. Peng, J. Shu, C. Li, X. Jiang, Q. Zhang, Adsorption behavior of methylene blue onto waste-derived adsorbent and exhaust gases recycling, RSC Adv. 7 (2017) 27331–27341, https://doi.org/10.1039/c7ra01482a.
[72] Y. Tao, B. Yang, F. Wang, Y. Yan, X. Hong, H. Xu, M. Xia, F. Wang, Green synthesis of MOF-808 with modulation of particle sizes and defects for efficient phosphate sequestration, Sep. Purif. Technol. (2022), 121825, https://doi.org/10.1016/j.seppur.2022.121825.
[73] F. Hashemzadeh, M. Ariannezhad, S.H. Derakhshandeh, Evaluation of Cephalexin and Amoxicillin removal from aqueous media using activated carbon produced from Aloe vera leaf waste, Chem. Phys. Lett. 800 (2022), 139656, https://doi.org/10.1016/j.cplett.2022.139656.
[74] Z. Wang, S. Bin Kang, S.W. Won, Polyethylenimine-aminated polyvinyl chloride fiber for adsorption of reactive dyes from single and binary component systems: adsorption kinetics and isotherm studies, Colloids Surf. A Physicochem. Eng. Asp. 647 (2022), 128983, https://doi.org/10.1016/j.colsurfa.2022.128983.
[75] T.D. Dinh, M.N. Phan, D.T. Nguyen, T.M.D. Le, A.K. Nadda, A.L. Srivastav, T.N. M. Pham, T.D. Pham, Removal of beta-lactam antibiotic in water environment by adsorption technique using cationic surfactant functionalized nanosilica rice husk, Environ. Res. 210 (2022), 112943, https://doi.org/10.1016/j.envres.2022.112943.
[76] J. Rashid, R. Azam, R. Kumar, M. Ahmad, A. Rehman, M.A. Barakat, Sulfonated polyether sulfone reinforced multiwall carbon nanotubes composite for the removal of lead in wastewater, Appl. Nanosci. 9 (2019) 1695–1705, https://doi.org/10.1007/s13204-019-00953-2.
[77] L. Jiang, H. Yu, X. Zhou, X. Hou, Z. Zou, S. Li, C. Li, X. Yao, Preparation, characterization, and adsorption properties of magnetic multi-walled carbon nanotubes for simultaneous removal of lead(II) and zinc(II) from aqueous solutions, Desalin. Water Treat. 57 (2016) 18446–18462, https://doi.org/10.1080/19443994.2015.1090924.
[78] S. Chatterjee, I. Sivareddy, S. De, Adsorptive removal of potentially toxic metals (cadmium, copper, nickel and zinc) by chemically treated laterite: Single and multicomponent batch and column study, J. Environ. Chem. Eng. 5 (2017) 3273–3289, https://doi.org/10.1016/j.jece.2017.06.029.
[79] I. Lung, M. Stan, O. Opris, M.L. Soran, M. Senila, M. Stefan, Removal of Lead(II), Cadmium(II), and Arsenic(III) from aqueous solution using magnetite nanoparticles prepared by green synthesis with box–behnken design, Anal. Lett. 51 (2018) 2517–2529, https://doi.org/10.1080/00032719.2018.1446974.
[80] H. Zhang, F. Xu, J. Xue, S. Chen, J. Wang, Y. Yang, Enhanced removal of heavy metal ions from aqueous solution using manganese dioxide-loaded biochar: Behavior and mechanism, Sci. Rep. 10 (2020) 1–13, https://doi.org/10.1038/s41598-020-63000-z.